Environmental Modelling and Software 197 (2026) 106824

Contents lists available at ScienceDirect

Environmental Modelling and Software

journal homepage: www.elsevier.com/locate/envsoft

Ensemble deep learning towards high-resolution soil-moisture mapping for enhanced water management in California's Central Valley

Ali Azedou [a,b,e], Aouatif Amine [a], Said Lahssini [b], Gordon Osterman [c], Mauricio Arboleda-Zapata [c,e], Michael Cosh [d], Isaya Kisekka [e,*]

[a] National School of Applied Sciences, Ibn Tofail University, B.P 241, Kenitra, Morocco
[b] National School of Forestry Engineering, Salé, 11000, Morocco
[c] USDA-ARS Sustainable Agricultural Water Systems, Davis, CA, USA
[d] USDA ARS, Beltsville, MD, USA
[e] Land, Air and Water Resources Department, and Biological and Agricultural Engineering Department, University of California, Davis, USA

ARTICLE INFO

Keywords:
Deep learning
Soil-moisture downscaling
Water management
California's central valley
Ensemble modeling
SMAP satellite
Root-zone soil moisture

ABSTRACT

Soil moisture (SM) plays a vital role in both hydrological and agricultural processes and is critical for achieving groundwater sustainability in agriculture through demand management. NASA's Soil Moisture Active Passive (SMAP) satellite measures the SM across the Earth and provides data on both the surface and root zone SM but at a coarse spatial resolution of 9 km, thereby limiting detailed analyses. This study aimed to develop an optimized deep ensemble learning framework to downscale the resolution of SMAP observations of California's Central Valley from 9 km to 30 m for both the surface and root-zone SM. Sensitivity analysis was employed to identify key explanatory variables. The models were then combined into an ensemble DNN trained on multiscale SMAP data and validated against in-situ SM measurements. The results demonstrated that the ensemble model achieved the highest coefficients of determination (R^2) of 0.789 and 0.683 for surface and root-zone SM, respectively, with the lowest root mean square errors of 0.0281 and 0.0814 cm3/cm3, respectively, along with the highest NSE scores of 0.50 and 0.433, thereby reliably capturing spatial patterns and predictive accuracy. A sensitivity analysis identified precipitation, LST, topographic factors, land cover, and vegetation indices as key predictors for SSM, while organic matter, silt content, precipitation, and DEM were the most influential for RZSM. Seasonal analysis revealed distinct patterns linked to climate and management practices at a spatial resolution of 30 m, thereby capturing seasonal variations in soil moisture among major crops. Additionally, SM maps can be used to refine the estimated evapotranspiration resulting from applied irrigation water sourced from groundwater pumping, allowing for better monitoring of water use. SM can also be used to inform agronomic practices, such as delayed irrigation in early spring, which can reduce groundwater demand.

1. Introduction

Soil moisture (SM) data is critical for the sustainable management of groundwater in both hydrological and agricultural systems (Wang et al., 2019). Accurate SM measurements are essential for irrigation scheduling (Gu et al., 2021), flood and drought forecasting (Abelen et al., 2015), hydrological modeling of runoff and groundwater recharge (Mei et al., 2023), and groundwater demand management. In California, groundwater sustainability relies on two main strategies: water supply augmentation, such as managed aquifer recharge, and water-demand management, including water allocation and pumping restrictions. The latter often depends on remote sensing of the Evapotranspiration of Applied Water (ET_{aw}), which reflects variations in SM storage (Orang et al., 2013). For example, delaying the start of the irrigation season allows crops to utilize off-season soil water, reducing walnut irrigation demand by approximately 20 % (Shackel et al., 2021). Accurate estimation of off-season SM storage is therefore crucial for effective farming and water management. Moreover, the availability of SM data at multiple spatial scales enhances both land and water resource planning (Sanchez-Mejia et al., 2014).

The Soil Moisture Active Passive (SMAP) satellite, launched by NASA in 2015, provides global SM observations every 2–3 days (Entekhabi et al., 2010). Its measurement system initially combined radar and

* Corresponding author.
E-mail address: ikisekka@ucdavis.edu (I. Kisekka).

https://doi.org/10.1016/j.envsoft.2025.106824
Received 25 February 2025; Received in revised form 16 October 2025; Accepted 4 December 2025
Available online 5 December 2025
1364-8152/© 2025 The Authors. Published by Elsevier Ltd. This is an open access article under the CC BY license (http://creativecommons.org/licenses/by/4.0/).

Abbreviations

CHIRPS	Climate Hazards Group Infrared Precipitation with Station
CNN	Convolutional neural network
CRNP	Cosmic-ray neutron probes
DEM	Digital elevation model
DL	Deep learning
DNN	Deep neural network
ET	Evapotranspiration
ET_{aw}	Evapotranspiration of applied water
GLDAS	Global Land Surface Assimilation System
LSTM	Long short-term memory
MODIS	Moderate Resolution Imaging Spectroradiometer
NDVI	Normalized difference vegetation index
NDWI	Normalized difference water index
NMR	Nuclear magnetic resonance
NSE	Nash-Sutcliffe Efficiency
RMSE	Root mean square error
RNN	Recurrent neural networks
RZSM	Root-zone soil moisture
SAR	Synthetic aperture radar
SGMA	Sustainable Groundwater Management Act
SM	Soil moisture
SMAP	Soil Moisture Active Passive
SMOS	Soil Moisture and Ocean Salinity
SSM	Surface soil moisture
TDR	Time-domain reflectometer
VIC	Variable infiltration capacity

radiometer sensors to capture SM in the top 5 cm of soil, but the radar component failed shortly after launch. Despite this, the SMAP Level-3 enhanced product continues to deliver SM estimates at a nominal 9-km resolution by downscaling passive radiometer observations using a blend of historical radar data, land-surface modeling, and ancillary datasets (Colliander et al., 2022). Several studies have confirmed that SMAP offers higher-resolution measurements than other coarse SM products (Zhang et al., 2017). For instance, Mazzariello et al. (2023) benchmarked SMAP against in-situ networks across European ecoregions and found smaller errors than the Advanced Scatterometer (ASCAT) and Soil Moisture and Ocean Salinity Centre (SMOS) products. Likewise, under dense vegetation, SMAP estimates outperform model-based products such as the fifth generation of European Centre for Medium-Range Weather Forecasts (ECMWF) (ERA5) and the Global Land Surface Assimilation System (GLDAS), as shown through triple collocation analysis (Kim et al., 2020). This blended approach allows SMAP to better capture spatial and temporal SM variations; however, it remains limited by model-dependent errors from ancillary datasets (Deng et al., 2022) and by vegetation water content interference, which can attenuate microwave signals and underestimate SM (Fan et al., 2020). However, the coarse 9–36 km resolution does not fully capture subpixel heterogeneity caused by topography, soil type, or vegetation (Chan et al., 2016; Fan et al., 2020), constraining its use in fine-scale hydrological modeling, irrigation management, and groundwater-demand planning (Sahaar and Niemann, 2020; Carranza et al., 2021; Wannasin et al., 2021).

Various approaches have been developed to downscale coarse-resolution soil moisture (SM) data, ranging from physically based land-surface models to statistical and hybrid methods. Physically based models, such as the Variable Infiltration Capacity (VIC), Noah, and the Community Land Model (CLM), simulate hydrological processes to generate finer-scale SM estimates for both surface and root zones (Shrestha et al., 2018; Rouf et al., 2021; Verhoest et al., 2015). While these models can capture local-scale variability when forced with satellite observations, they typically operate at coarse resolutions of 10–100 km, which may obscure sub-grid heterogeneity. Structural simplifications in processes like infiltration, runoff, vegetation dynamics, soil layering, and snowpack representation can lead to persistent errors and unrealistic transitions between grid cells (Glotfelty et al., 2021; He et al., 2023).

To address these limitations, statistical and hybrid downscaling approaches have been applied. Statistical methods establish relationships between coarse and fine-scale SM data, while data assimilation techniques, such as ensemble Kalman filters, dynamically update fine-scale model states based on observations (Sahoo et al., 2013; Peng et al., 2017). Notably, models like EMT + VS integrate topography, soil, and vegetation influences to produce high-resolution SM maps (10–40 m), outperforming other methods in capturing spatial variability (Deshon et al., 2020; Fischer et al., 2025). Overall, downscaling techniques span a spectrum from simple empirical methods to complex process-rich frameworks, each with distinct strengths and limitations for improving the spatial and temporal detail of soil moisture.

Another widely used approach is scale-invariant downscaling, which relies on the assumption that the relationships between the target variable (e.g., SM) and conditioning factors remain consistent across scales (Tang et al., 2021; Wu et al., 2022). This method trains predictive models on data resampled to increasingly coarse resolutions and then applies them to native or full-resolution ancillary layers to generate fine-scale predictions. Additionally, its effectiveness has been demonstrated in prior SM-data-downscaling studies (Qu et al., 2021; Zhao et al., 2022; Nadeem et al., 2023). Although the advantages of scale-invariant downscaling have been validated, some studies have questioned its underlying assumption that factor–target relationships are fully consistent across various scales (Shangguan et al., 2023). Qu et al. (2021) noted an overall decline in the downscaling accuracy compared to that of the original microwave products. Subsequently, Nadeem et al. (2023) compared downscaled and native-scale SM data and found that although some methods were better at preserving patterns, their prediction accuracy generally declined with scale. These limitations are particularly evident in heterogeneous landscapes or during seasonal extremes, where the scale-invariant assumptions underlying multifractal downscaling (Park et al., 2019; Kofidou et al., 2023) may not fully capture the relationships between soil moisture and predictors. Furthermore, Zhao et al. (2022) demonstrated that scale effects vary among convolutional neural network (CNN) models, with the residual network (ResNet) model minimizing their impact through residual corrections.

California's Central Valley is a highly productive agricultural region facing increasing water challenges due to its Mediterranean climate, characterized by hot, dry summers that create soil moisture deficits for crop irrigation, further exacerbated by climate change. Recurring multiyear droughts have depleted surface-water supplies and mountain snowpacks, leading to heavy groundwater extraction, aquifer overdrafts, and regional subsidence (Gaeta, 2021). To address these issues, the Sustainable Groundwater Management Act (SGMA), enacted in 2014, requires the formation of Groundwater Sustainability Agencies (GSAs) for high- and medium-priority basins, classified based on factors such as overdraft risk, population dependence, and water availability. These GSAs develop and implement Groundwater Sustainability Plans (GSPs) to mitigate overdraft and avoid undesirable results within 20 years. Improved soil moisture monitoring supports agricultural resilience by enabling optimized water-demand management and irrigation scheduling (DWR, 2021). Some GSAs use ETaw, the evapotranspiration from applied irrigation water, calculated as the portion of actual ET attributable solely due to irrigation (DeJonge et al., 2025) to track water allocation and over-pumping. However, high-resolution soil moisture data are needed to refine ETaw estimates. In this context, this study aims to evaluate an optimized deep ensemble learning framework to downscale SMAP soil moisture to 30-m resolution, capturing nonlinear relationships across multiple scales and identifying the most influential ancillary predictors.

To build upon the recent progress in addressing the scale-effect uncertainties in SM data, this study makes the following contributions:

1) It developed a novel framework for downscaling surface soil moisture (SSM) and root-zone soil moisture (RZSM) to 30 m through an ensemble DL architecture comprising deep neural network (DNN), CNN, and long short-term memory (LSTM) models trained in a multiscale manner (1000, 100, and 50 m).
2) A sensitivity analysis of ancillary predictors was conducted to evaluate the relative importance of each variable for clarifying the SM.
3) A Bayesian optimization method was proposed to determine optimized neural network (NN) architectures tailored for SM-data downscaling.
4) The proposed ensemble model was employed to simulate seasonal changes in SSM and RZSM over 2023–2024, with particular emphasis on evaluating plant-available water in the root zone at the end of winter to inform early-season irrigation planning (i.e., to inform delayed initiation of irrigation in spring).

2. Study area and datasets

2.1. Study area

Encompassing approximately 51,800 km^2, the Central Valley of California is located between the Sierra Nevada Mountains and its coastal ranges. It comprises highly productive agricultural land that accounts for approximately 20 % of irrigated land and groundwater demand in the United States (Li et al., 2018). It features a Mediterranean climate with hot, dry summers and cool, wet winters. The average annual precipitation ranges from over 864 mm in Redding, CA, to less than 165 mm in Bakersfield, CA, which is located in the southern part of the Central Valley, with over 80 % of the precipitation occurring as rain between November and April (LaDochy and Witiw, 2023). The summers are characterized by high temperatures and little to no rainfall, creating SM deficits that considerably affect crop growth. The fertile soils of the Central Valley and the extensive water-supply infrastructure enable diverse irrigated agriculture, which is vital for both the state and national food supply (May-Lagunes et al., 2023). However, overreliance on unsustainable groundwater extraction to buffer surface-water shortages during droughts puts the agricultural sector and hundreds of thousands of jobs at long-term risk.

The region produces a wide variety of high-value crops, including almonds, pistachios, grapes, citrus tomatoes, and alfalfa, as well as major livestock feed for California's dairy and beef industries (Sumner, 2014). The southern San Joaquin Valley alone accounts for over 50 % of the nation's fruit, vegetable, and nut production (Escriva-Bou et al., 2023), generating over 17$ billion in annual revenue and supporting hundreds and thousands of jobs (Faunt. 2009). However, the valley faces growing water-resource challenges due to its semi-arid climate, intensive irrigation demands, and periodic droughts that reduce surface water availability and drive unsustainable groundwater extraction (Howitt et al., 2014; Holmes, 2023). Persistent groundwater declines have led to land subsidence and difficulty in meeting the Sustainable Groundwater Management Act (SGMA) goals (Babbitt et al., 2018). Strengthening groundwater and irrigation management practices is therefore essential to sustaining agricultural productivity and water resilience under climate change conditions.

2.2. Datasets

2.2.1. Satellite SM dataset

The SMAP satellite, launched by NASA in 2015, provides global SM observations every 2–3 days at a depth of ~5 cm. It's radiometer measures the brightness temperature at native resolution of 36 km. SMAP data products are distributed across four processing levels. Level 1 contains calibrated and geolocated brightness temperature observations. Level 2 and 3 products differ by scale, with Level 2 providing half-orbit retrievals and Level 3 offering daily global composites. Level 4 (L4) includes global SM observations of the surface (0–5 cm) and root zone (0–100 cm) with a 9 km spatial resolution, including surface meteorological variables, soil temperature, ET, and net radiation measurements. In this study, SMAP L4 data were acquired from November 1 to December 5, 2023, matching the period of available in-situ observations for validation. The L4 product assimilates SMAP radiometer brightness temperature observations into the NASA Catchment Land Surface Model at 6 a.m. and 6 p.m. local time using a 9-km Equal-Area Scalable Earth Grid (EASE-Grid). The dataset was accessed through Google Earth Engine, where it is represented at a nominal resolution of approximately 11 km owing to internal gridding.

2.2.2. Ancillary data

This study employed 20 high-resolution auxiliary datasets, including the synthetic aperture radar (SAR) backscatter from the VH and VV bands of Sentinel-1, precipitation from Climate Hazards Group Infrared Precipitation with Station data (CHIRPS), land-surface temperature from MODIS, vegetation indices from Sentinel-2, digital elevation data, derived terrain variables, and soil parameters, as listed in Table 1 and visualized in Fig. S1, as predictor variables for downscaling the SMAP SM data of Central Valley, California. Except for the digital elevation model (DEM) and soil properties, all datasets were sampled to the spatiotemporal extent of the study area and the period of interest.

3. Methods

In this study, we developed and evaluated an ensemble DL modeling framework for downscaling the SMAP for SSM and RZSM, as shown in Fig. 1. The methodology involved acquiring and preprocessing satellite, in-situ, and ancillary datasets, optimizing three base DL models using Bayesian hyperparameter tuning, and combining their outputs into an ensemble model. A sensitivity analysis was then conducted to determine the most relevant predictors, followed by validation against in situ SM measurements using several statistical metrics. This methodology was followed to exploit complementary strengths of individual DL models to enhance SM downscaling accuracy.

3.1. Data preprocessing

The data in Table 1 were resampled to 1000 × 1000 m, 100 × 100 m, 50 × 50 m, and 30 × 30 m to prepare the training and contextual data for the downscaling model. Cubic interpolation was used for its efficiency and ability to preserve spatial continuity across scales. Soil property layers were also aggregated from their native 30 m to coarser resolutions to ensure consistency across inputs.

This multi-resolution approach enhanced model robustness by enabling the deep learning framework to learn spatial relationships at different scales. Training labels at each resolution corresponded to SMAP values at the same scale. To capture seasonal variability, the model was trained on a full hydrologic year (May 2023–March 2024) of SMAP L4 data, encompassing both wet and dry periods.

All features were standardized (mean = 0, SD = 1) to ensure balanced learning, and the data were split spatially into 70 % for training and 30 % for testing to maintain independence. A 10-fold cross-validation scheme was applied across all models to optimize performance.

Table 1
Datasets used as predictor variables for downscaling SMAP SM data of the Central Valley, California.

Type	Variable	Dataset ID	Spatial resolution	Data source	Reference	Periods
Target variables	Surface SM	NASA/SMAP/SPL4SMGP/007	11000 m	NASA Jet Propulsion Laboratory	Reichle et al. (2022)	05/01/2023–03/31/2024
	RZSM					
Meteorological	Precipitation	UCSB-CHG/CHIRPS/DAILY	5566 m	CHIRPS (V2)	Funk et al. (2015)	11/01/2023–12/05/2023
	ET	MODIS/061/MOD16A2	500 m	NASA LP DAAC at the USGS EROS Center	Running et al. (2021)	11/01/2023–12/05/2023
	Land Surface Temperature	MODIS/061/MOD11A2	1000 m			11/01/2023–12/05/2023
Topographic	Elevation	USGS/3DEP/10m	10.2 m	United States Geological Survey	–	May 06, 2020
	Slope					
	Topographic Wetness Index					
SAR data	Backscatter	COPERNICUS/S1_GRD	10 m	European Union/ESA/Copernicus	–	11/01/2023–12/05/2023
Vegetation indices	NDVI	COPERNICUS/S2_SR_HARMONIZED	10 m		–	
	Soil-adjusted Vegetation Index					
	NDWI					
	Leaf Area Index					
	Enhanced Vegetation Index					
Land use/Land cover	Crop	USDA/NASS/CDL	30 m	United States Department of Agriculture	Alemu et al. (2019)	January 01, 2023
	Land Cover	GOOGLE/DYNAMICWORLD/V1	10 m	Google Earth	Brown et al. (2022)	11/01/2023–12/05/2023
Soil properties	Organic Matter	PROJECTS/SAT-IO/OPEN-DATASETS/POLARIS	30 m	Probabilistic Remapping of SSURGO (POLARIS)	Chaney et al. (2019)	January 05, 2019
	Bulk Density					
	Sand Percentage					
	Silt Percentage					
	Clay Percentage					

NDVI: normalized difference vegetation index; NDWI: normalized difference water index.

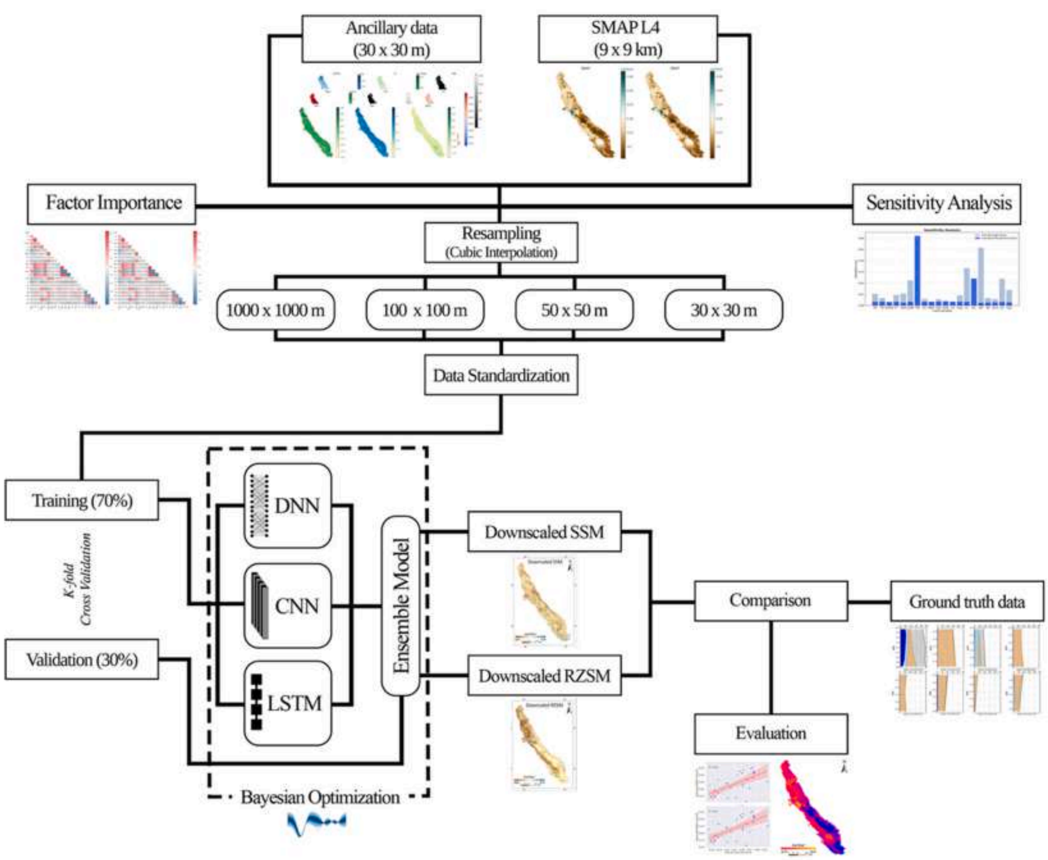

Fig. 1. Overview of the proposed ensemble SM-data downscaling framework.

3.2. SM measurements

To validate the downscaled SMAP data, three field-SM measurement expeditions were undertaken between November 3, 2023, and December 5, 2023; the locations are shown in Fig. 2.

In the first field-SM measurement expedition, shown in Fig. 2(a), measurements were obtained from 27 sites spanning the Central Valley and Sierra Nevada regions of California using a portable nuclear magnetic resonance (NMR) probe (Walsh et al., 2013). These included single-point logs collected during the expedition. The NMR proton is widely recognized as a direct method for measuring SM content. The probe applies radiofrequency pulses that are tuned to the resonance frequency of hydrogen protons in the porous media. These pulses excite the protons and cause them to emit a measurable signal that decays as the protons relax back to equilibrium. The initial signal magnitude correlates with the number of excited protons and, therefore, the total water content in the sensitivity zone. NMR measurements do not require site-specific calibration due to their direct sensitivity to groundwater. The signal-decay rate varies with water distribution in the soil matrix. The Dart NMR probe (Vista Clara, Mukilteo, WA, USA) was used for SM measurements from polyvinyl chloride access tubes with a diameter of 5 cm that were installed at depths ranging from 0.8 to 3.0 m. This enabled the collection of vertically resolved SM profiles of different ecosystems, examples of which are shown in Fig. S2.

In the second field-SM measurement expedition, shown in Fig. 2(b), time-domain reflectometer (TDR) sensors were deployed across 54 sites throughout the Central Valley to monitor near-surface volumetric SM passively. The TDR sensors comprised parallel metal rods inserted vertically into the soil pits and connected to an SM sensor reader kit (SDI-12; Acclima, Meridian, ID, USA). The sensors recorded single-time measurements during the expedition period by measuring the travel time of a reflected waveform, which relates to the dielectric constant and, thus, the volumetric water content through factory calibration equations (Peddinti et al., 2020).

The third field-SM measurement expedition aimed to test the temporal stability of the downscaling method, specifically its accuracy in downscaling soil moisture across different time periods. This investigation focused on the impact of cover crops on soil moisture dynamics in a young pistachio orchard in the northern Central Valley near Woodland, CA. Continuous hourly measurements were obtained between May 2023 and March 2024. At this site, soil moisture was measured using a neutron probe (CPN 503 Hydroprobe Elite; InstroTek, San Francisco, CA, USA) with a measurement range of 0–6 in/ft. To deploy the neutron probe, 3.6 m long aluminum access tubes with a diameter of 38 mm were manually installed at eight locations using a hand auger, and soil samples were collected during the installation. The wet samples were first weighed and then oven-dried at 105 °C and weighed again to determine their gravimetric water content, which was used to calibrate the neutron probe for the local soil types through relationships established between the neutron counts and volumetric water content. The probe readings for the cover and non-cover-crop areas of each field were analyzed individually.

Additionally, soil moisture was monitored using two cosmic ray neutron probes (CRNPs). A 3He thermal neutron detector (HydroSens, Lab-c, Sheridan, WY, USA) provided continuous in-situ SM monitoring in the orchard. These probes measure SM by detecting changes in neutron flux caused by cosmic rays interacting with hydrogen nuclei in soil water. Cosmic rays generate secondary particles, including fast neutrons, which are moderated by hydrogen molecules in the soil (Babaeian et al., 2019). The CRNP detects reductions in fast neutrons, correlating with SM content, as more hydrogen (from water) decreases neutron counts. This non-invasive method allows for continuous SM measurements over large areas, aiding agricultural irrigation management and hydrological studies. Further details on the CRNP design used in this study can be found in Zreda et al. (2012).

All in-situ SM measurements underwent quality-control procedures to eliminate erroneous values from sensor malfunctions or data collection errors. For example, improper standard count settings in the

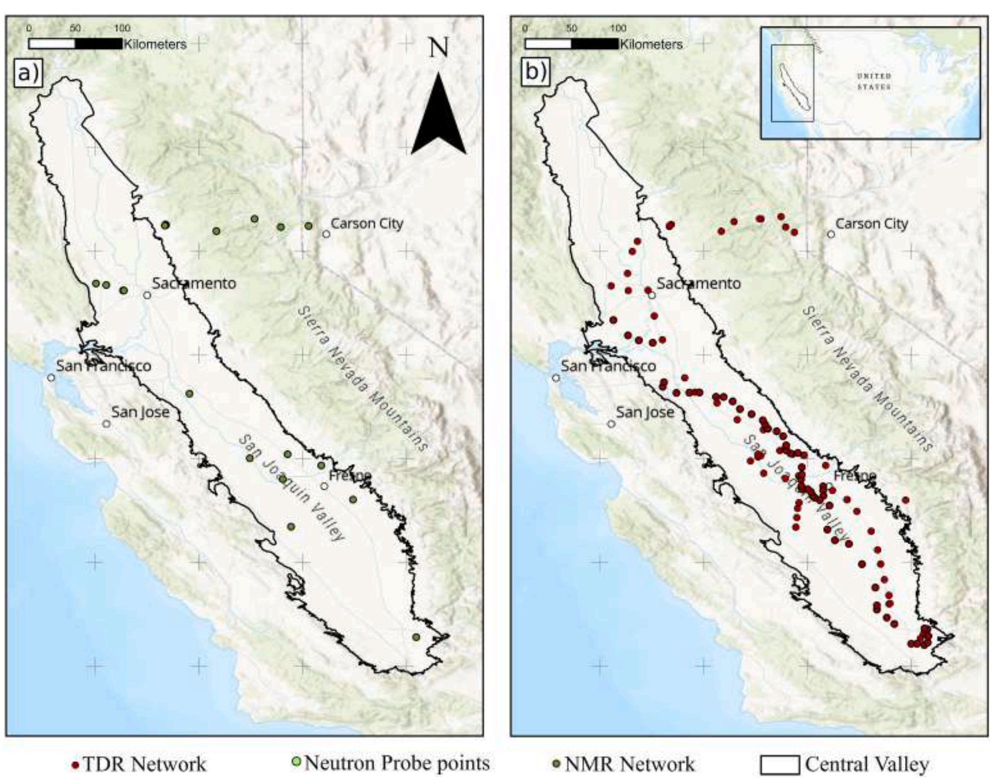

Fig. 2. Location of the field SM measurement expeditions undertaken in the Central Valley, California. (a) First expedition, (b) second expedition. TDR: time-domain reflectometer; NMR: nuclear magnetic resonance.

neutron probe can lead to inaccuracies (Bell, 1987). When downscaled satellite rasters were available, valid measurements matching the SMAP overpass dates/times were extracted. These measurements, retained at their native scale, were compared directly to the downscaled 30-m-resolution SMAP rasters from the same dates to assess model performance in mapping high-resolution SM data.

The sensitive volumes of each measurement ranged from approximately 5 cm for the TDR sensors to 25 cm for the NMR probe logs and to a larger scale for the CRNP (effective radius of approximately 150 m). For the root-zone SMAP (0–100 cm), the NMR and CRNP data were averaged across probe depths in the upper 1 m.

To ensure meaningful comparisons between in-situ soil moisture observations and downscaled SMAP data at 30 m resolution, we applied a depth- and footprint-aware matching approach. TDR sensors were directly matched to the 30 m SMAP downscaled pixels, assuming minimal depth mismatch. Spatially, we assigned each point measurement to the nearest 30 m pixel centroid without interpolation, noting that these sensors inherently reflect highly local conditions. NMR sensors provide point measurements of soil moisture to a depth of 3 m. We followed a similar approach to TDR to compare NMR-measured soil moisture in the top 1 m to the 30 m downscaled soil moisture. Average soil moisture in the top 1 cm was compared to the downloaded SMAP soil moisture, similarly to NMR. For CRNP, which integrates soil moisture over a broader footprint (~150 m radius, 0–80 cm depth), all downscaled SMAP pixels were averaged within a 150 m buffer to match its spatial scale.

3.3. Model development

This study used the scale-invariant assumption that the relationship between SM and auxiliary surface parameters does not change across different scales (Jiang et al., 2017). Based on this assumption, the associations determined from low-resolution conditioning data can be plausibly extended to derive high-resolution SM estimates by utilizing the corresponding fine-scale covariate layers. To test the viability of this assumption for our downscaling task, three DL models were developed: DNN, CNN, and LSTM.

The DNN served as a baseline model to capture nonlinear relationships between SM and the input predictors. The CNN was used to extract spatial patterns from gridded covariate stacks, including longitude, latitude, and stacked environmental factors. The LSTM network was employed to model temporal dependencies in sequential SM data, addressing potential time-lagged relationships.

Finally, an ensemble model was created by combining the DNN, CNN, and LSTM models to leverage their complementary strengths. The ensemble architecture was optimized in the same manner. It was trained on different-resolution data, and its performance for downscaling the SMAP SM data was validated.

Detailed descriptions of the network architectures, training procedures, and model hyperparameters are provided in the Supplementary Materials (Fig. S3–S6).

3.4. Hyperparameter tuning

A key step for developing effective DL models is to optimize their architectures to best capture the predictive relationships from the input data. In this study, Bayesian optimization was employed to automatically tune the hyperparameters of both the base DL models and the ensemble architecture. Bayesian optimization treats hyperparameter tuning as a black-box optimization problem and builds a probabilistic model of model performance as a function of the hyperparameters (Victoria and Maragatham, 2021; Sbahi et al., 2025). It balances the exploration of new configurations by exploiting prior knowledge to converge to optimal values efficiently (Azedou et al., 2023).

In this study, the hyperparameters were simultaneously tuned via Bayesian optimization over 50 iterations, and the optimized hyperparameters are listed in Table 2. Additionally, the ten-fold cross-validation performance on the training set was optimized, which facilitated the automatic process of proposing architectures, evaluating reserved data, and updating the probabilistic model to recommend enhanced hyperparameters. The optimized structures depicted in Fig. 5 demonstrate the efficacy of Bayesian optimization for navigating intricate design spaces to develop customized DL models.

3.5. Sensitivity analysis

A factorial sensitivity analysis was conducted to assess the relative contribution of each input variable (Table 1) to the ensemble model's downscaling performance (Anbarasu et al., 2020). Each of the 20 explanatory variables was systematically omitted in turn, and model performance was re-evaluated using the validation RMSE to quantify its marginal influence. Differences between the complete and reduced models indicated the sensitivity of the downscaling process to each variable.

The goal was not to remove correlated features but to identify those with limited marginal utility. Deep learning models are inherently robust to multicollinearity through nonlinear transformations, feature abstraction, and regularization (Chan et al., 2022; Lindner et al., 2022). Therefore, correlated yet informative variables were retained to support generalization. The analysis helped highlight the most influential covariates and identify those whose exclusion caused negligible performance loss, thereby guiding potential model simplification.

3.6. Model performance

The model performance was quantified using five commonly employed statistical metrics computed between each in-situ measurement and its matching downscaled retrieval (Entekhabi et al., 2010; Zhao et al., 2022): the Pearson correlation coefficient (R), root mean square error (RMSE), bias, unbiased RMSE (ubRMSE), and the Nash-Sutcliffe Efficiency (NSE). These metrics are defined as follows:

$$R = \frac{1}{N-1}\sum_{i=1}^{N}\left(\frac{x_i-\overline{x}}{\sigma_x}\right)\left(\frac{y_i-\overline{y}}{\sigma_y}\right)$$

$$RMSE = \sqrt{\frac{1}{N}\sum_{i=1}^{N}(x_i-y_i)^2}$$

$$Bias = \frac{1}{N}\sum_{i=1}^{N}(x_i-y_i)$$

$$ubRMSE = \sqrt{(RMSE^2 - Bias^2)}$$

$$NSE = 1 - \frac{\sum_{i=1}^{N}(x_i-y_i)^2}{\sum_{i=1}^{N}(x_i-\overline{y}_i)^2}$$

where x_i and y_i denote the downscaled observations and ground-truth data, respectively; N denotes the number of observations; $\overline{x}_i$ and $\overline{y}_i$ are the averages of x_i and y_i, respectively; σ_x and σ_y represent the standard deviations of $\overline{x}_i$ and $\overline{y}_i$, respectively, and R is the consistency between datasets. Bias and RMSE indicate the downscaling accuracy, with lower values reflecting better precision. Additionally, ubRMSE represents the true variation between the data sources after removing the bias effects. Finally, the NSE assesses the predictive skill of the model by comparing its performance to that of the mean of the observations. An NSE value of 1 indicates perfect agreement, 0 indicates no improvement over using the mean of observations, and values below 0 suggest poor predictive performance.

Table 2
Hyperparameters optimized via Bayesian optimization for the ensemble DL model.

DNN and Ensemble Model				CNN				LSTM			
Hyperparameter	Min	Max	Step	Hyperparameter	Min	Max	Step	Hyperparameter	Min	Max	Step
Number of layers	1	16	1	Number of convolutions	1	4	1	Number of LSTM layers	1	16	1
Number of nodes	32	1024	32	Number of filters	32	256	16	Number of units	32	256	16
				Kernel size	3	5	1	Dropout	0.1	0.5	0.1
				Pooling size	2	4	1				
				Number of dense layers	1	16	1				
				Number of nodes	32	1024	32				
Activation functions	ReLU, tanh, sigmoid, ELU[a], softmax, exponential										

[a] ELU: Exponential linear unit.

3.7. Available water content calculation

To evaluate plant-available water in the root zone at the end of the winter season, we developed a spatial map using the downscaled RZSM data and soil physical properties from POLARIS. The plant-available water content (AWC) at the end of winter was calculated as:

$$AWC = (\theta e - \theta pwp) \times Drz$$

where AWC is the available water content (mm/m) at the end of the winter season, θe is the ensemble-modeled RZSM at the end of winter (March 21, 2024), θpwp is the permanent wilting point (m^3/m^3), and Drz is the root zone depth (1000 mm).

The permanent wilting point (θpwp) was calculated using a two-step process (Saxton and Rawls, 2006). The first solution is the permanent wilting point ($PWPt$) determined using soil texture and organic matter data:

$$PWPt = -0.024S + 0.487C + 0.006OM + 0.005(S \times OM) - 0.013(C \times OM) + 0.068(S \times C) + 0.031$$

where S is the sand content (%), C is the clay content (%), and OM is the organic matter content (%). The final permanent wilting point was then adjusted using:

$$\theta pwp = PWPt + (0.14 \times PWPt - 0.02)$$

4. Results

4.1. Sensitivity analysis

Fig. 3 presents the correlation matrices of the associations between the SM data and the explanatory variables.

The correlation matrix of SSM revealed both expected and insightful relationships between the SSM data and the explanatory variables. The SMAP SM correlated reasonably well with precipitation, LST, and some vegetation indices, such as the normalized difference water index (NDWI), with a 0.47 correlation coefficient, demonstrating the influence of these factors, as anticipated. Topographic parameters, such as those from the DEM and slope, exhibited inverse associations with a respective correlation coefficient of −0.55 and −0.21, indicating the influence of elevation and topography. Crop and LC showed high correlation with the SSM, indicating a high influence of the anthropogenic activities on the SM. The sentinel backscatter bands VH and VV were closely correlated, as expected for related microwave observations, with VH also exhibiting a moderate relationship with ET and NDVI, indicating the effects of surface roughness and vegetation. Generally, stronger correlations existed between the SM data and both topographic and vegetation indices compared to soil covariates, implying that surface conditions exert stronger control over near-surface moisture than subsurface properties.

Furthermore, the RZSM correlation matrix revealed weaker relationships between RZSM and climatic or vegetation factors than those with SSM, with more moderate correlations between the CHIRPS and NDWI data. However, the topography exhibited clear relationships, as DEM and TWI were negatively correlated with RZSM, presenting respective correlation values of −0.46 and −0.25, potentially reflecting the subsurface infiltration pathways. Soil texture parameters, notably the organic-matter content, were more distinctly and positively correlated with the RZSM than with SSM, with a correlation value of −0.39, implying that deeper moisture storage was influenced more by lithologic controls compared with infiltration and water-holding capacity. Overall, the results reinforced the assumption that root-zone patterns differ from those of the surface layers and are governed more by terrain attributes related to rainfall penetration and subsurface composition than near-surface climatic drivers.

Fig. 4 depicts the results of the sensitivity analysis, which shows the RMSE obtained by excluding various factors during SSM and RZSM downscaling.

Sensitivity analysis effectively evaluated the influence of each explanatory variable on the SSM downscaling performance. Precipitation (CHIRPS), DEM, NDVI, and soil-adjusted vegetation index were among the most impactful, resulting in RMSE of >0.15 cm^3/cm^3 when omitted from the model. NDWI also exhibited high sensitivity, reflecting its role in capturing near-surface moisture dynamics. Furthermore, variables such as VH, VV, ET, land-surface temperature, and crop/land cover exhibited more modest effects on RMSE, suggesting that they had a secondary influence on surface patterns related to topographic and vegetation factors. This analysis clarified the key physical drivers governing the variability in near-surface SM distribution across the Central Valley.

Additionally, the sensitivity analysis showed that organic matter and silt percentage had the strongest effect on the downscaling of RZSM, with their exclusion leading to RMSE of more than 0.15–0.25 cm^3/cm^3. Precipitation and DEM were also influential; however, the effects of other terrain and vegetation covariates on deep SM were lower than those for SSM. This reinforces the notion that subsurface SM patterns are governed more by soil characteristics related to water storage and drainage capacity. Thus, this analysis effectively identified lithological properties as the primary physical controls of the RZSM distribution compared with near-surface climatic drivers.

4.2. Evaluation of the SM-data downscaling framework

As shown in Fig. 5, Bayesian optimization allowed us to determine the overall architecture of the optimized DL ensemble model.

The base DNN comprised 17 densely connected layers with varying node counts and activation functions for complex nonlinear mapping of the input data. The CNN employed 1D convolutional filtering, followed by max pooling, to automatically extract the spatial patterns from the data, whereas the LSTM incorporated memory gates within an initial layer of 256 units, subsequent layers of 32 units each, and a dropout layer to capture the temporal dependencies in the input sequences. These specialized model outputs were then fed into the ensemble DL model, which comprised six densely connected combiner layers, with node counts ranging from 192 to 288. Additionally, nonlinear activation

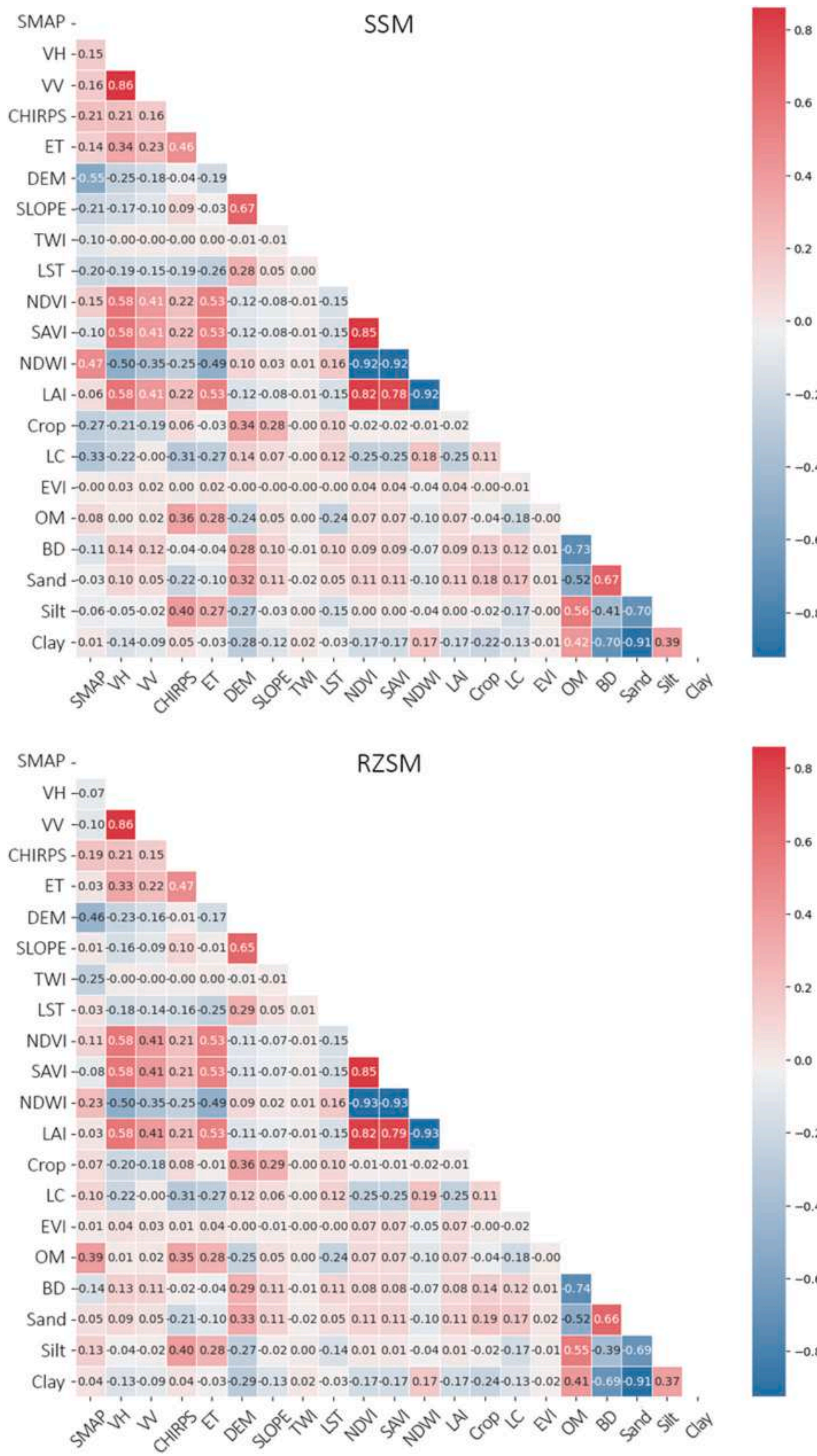

Fig. 3. Correlation matrices of surface soil moisture (SSM), root zone soil moisture (RZSM), and explanatory variables.

functions, including tanh, ReLU, and softmax, were employed within the dense layers. Finally, a 0.2 dropout layer was included to prevent overfitting.

The performance of each model for downscaling the SSM and RZSM data was quantified using the four statistical evaluation metrics, whose values were calculated by comparing the downscaled maps and corresponding ground observations; the results of each model are presented in Table 3.

For SSM-data downscaling, the ensemble model achieved the highest R-value of 0.789, indicating the strongest linear correlation with the

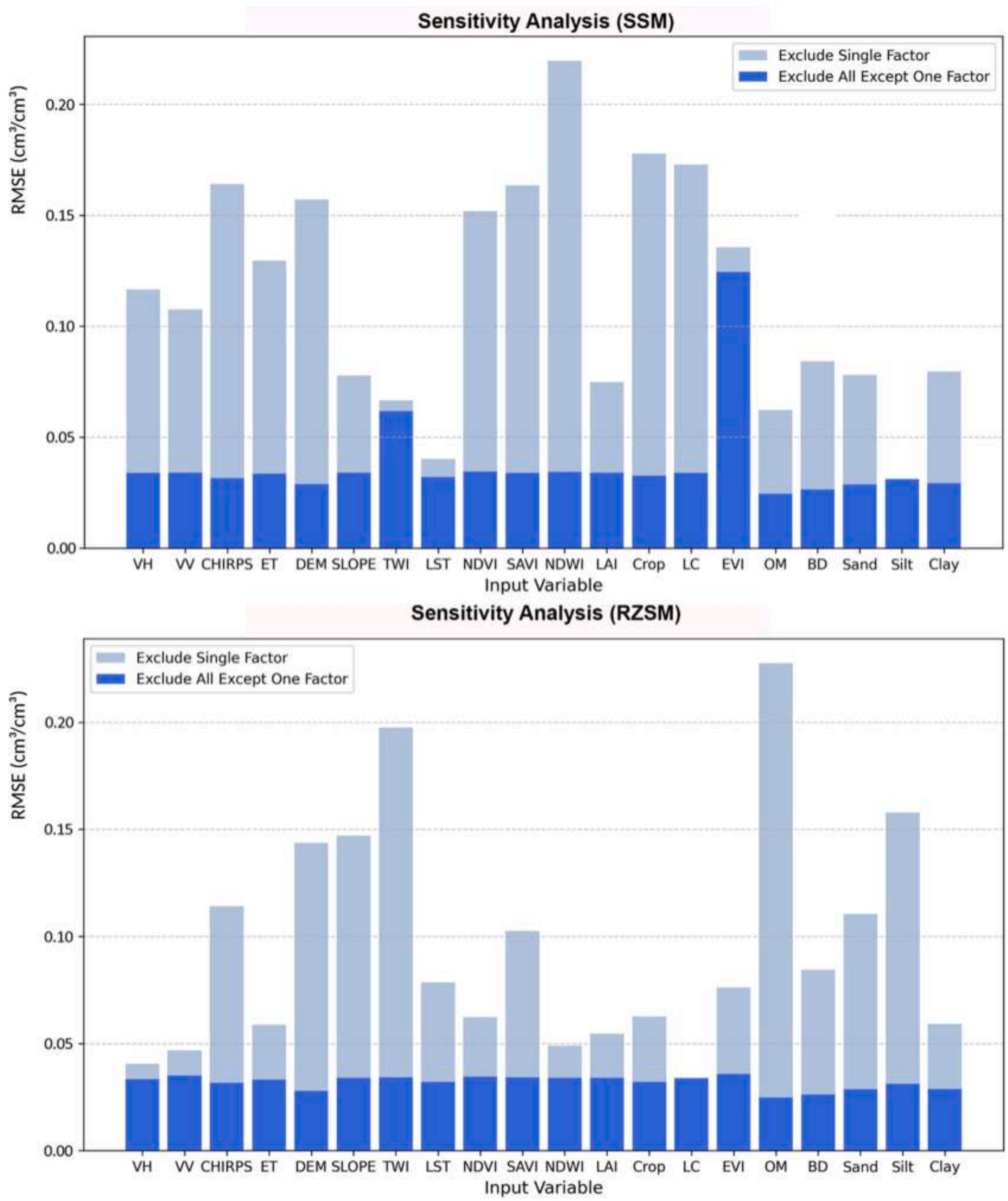

Fig. 4. Sensitivity analysis of explanatory variables for downscaling surface soil moisture (SSM) and root zone soil moisture (RZSM) data.

observations. It also exhibited the lowest bias and RMSE, thereby demonstrating the highest accuracy for capturing spatial patterns in the near-surface SM data. In terms of NSE, the ensemble model again outperformed the individual models, attaining the highest NSE value of 0.50, which indicates a substantially improved predictive skill over the baseline mean-observation model.

Additionally, the LSTM model showed the lowest R-value, highest RMSE, and lowest NSE, confirming limited predictive strength.

For RZSM-data downscaling, the ensemble model yielded the highest correlation (R = 0.6834), lowest bias, and second-lowest RMSE, while also achieving the highest NSE among all the models. Additionally, the LSTM model exhibited the poorest performance, as evidenced by its lowest R-value, NSE value, and highest ubRMSE among the other models. Overall, the ensemble model, which leveraged the complementary strengths of the individual DNN, CNN, and LSTM models, consistently outperformed the base models on most metrics. This suggests that it achieved the best performance balance for the large-scale downscaling of both the SSM and RZSM data, from coarse to fine resolutions, based on the multisource datasets employed. To further examine the model performance, correlation plots of the observed versus predicted SSM and RZSM data were generated using the calculated R^2 values (Fig. 6).

For SSM-data downscaling, the ensemble model achieved the highest R^2 value of 0.50, indicating that it captured the most variations in the observations, whereas the CNN, DNN, and LSTM models achieved lower R^2 values of 0.38, 0.41, and 0.35, respectively, indicating their weaker predictive powers for SSM. Additionally, the ensemble model also exhibited the best performance for RZSM-data downscaling, with an R^2 value of 0.43. The other models exhibited similar R^2 values ranging from 0.33 to 0.35, indicating a higher uncertainty for simulating deeper SM patterns than near-surface ones.

The higher R^2 values obtained by the ensemble model for both SSM

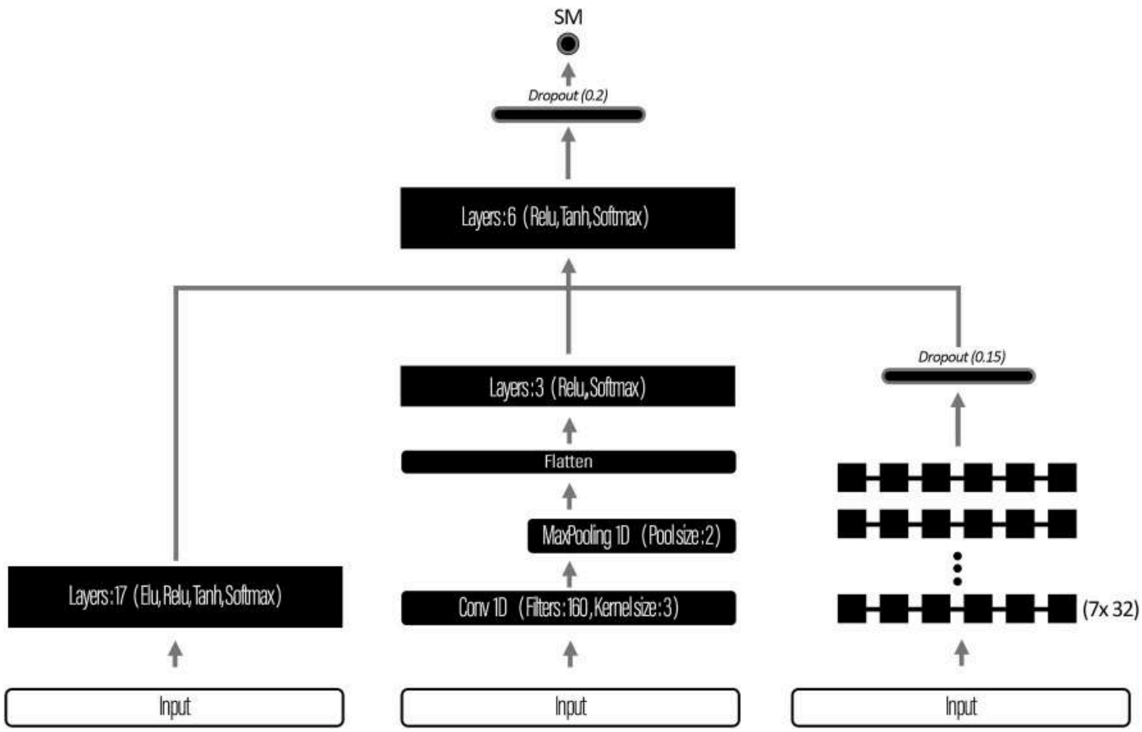

Fig. 5. Architecture of the ensemble DL model.

Table 3
Results of SSM and RZSM data downscaling for each model.

	SSM					RZSM				
	R	Bias (cm^3/cm^3)	RMSE (cm^3/cm^3)	UbRMSE (cm^3/cm^3)	NSE	R	Bias (cm^3/cm^3)	RMSE (cm^3/cm^3)	UbRMSE (cm^3/cm^3)	NSE
SMAP L4	−0.085	0.050	0.082	0.065	−1.38	0.143	0.0251	0.0651	0.0601	−0.4081
DNN	0.761	−0.011	0.029	0.026	0.408	0.6277	0.0147	0.0873	0.0861	0.350
LSTM	0.704	−0.009	0.032	0.030	0,352	0.6018	0.0059	0.0885	0.0883	0.332
CNN	0.712	−0.006	0.031	0.030	0.384	0.6441	0.0234	0.0871	0.0839	0.334
Ensemble	0.789	−0.011	0.028	0.025	0.500	0.6834	0.0035	0.0814	0.0814	0.434

and RZSM data, as evidenced by the correlation plots, further corroborate its enhanced performance for capturing the spatial distribution of not only the SSM, but also RZSM, than the individual models, thereby validating that it can be used for large-scale SM-data downscaling.

To gain further insights into the local characteristics and uncertainties within the SMAP data, the bias and RMSE for the original 9 km product and downscaled 30-m maps for both SSM and RZSM were spatially computed (Fig. 7). This facilitated direct point-to-point comparisons between the original coarse-resolution SM retrievals and downscaled maps, despite the differences in the native scale, yielding 30-m-resolution maps depicting the spatial patterns in bias and RMSE between the original SMAP products and downscaled maps across the entire study area.

The bias maps revealed distinct spatial patterns of both the SSM and RZSM between the northern and southern regions of the Central Valley. Specifically, the northern region exhibits predominantly positive biases of approximately 0.28 cm^3/cm^3, whereas the southern region exhibits negative biases of approximately -0.2 cm^3/cm^3. This suggests a systemic divergence in the SM representation of the original SMAP product across the study area. Notably, the ensemble downscaling approach mitigated these biases more effectively than the individual models for both the SSM and RZSM. Among the base models, DNN exhibited negligible bias, specifically for SSM, whereas CNN and LSTM exhibited comparable spatial biases. Additionally, the RMSE maps indicate lower errors of approximately 0.03 cm^3/cm^3 for the northern regions compared with 0.10 cm^3/cm^3 for the southern regions for both SSM and RZSM. Bias rectification through ensemble downscaling minimized the RMSE across the Central Valley. For the SSM, the DNN yielded marginally lower RMSEs than the other standalone models. However, the disparities between the standalone models were less evident for the RZSM. Overall, the spatial statistical metrics revealed systematic inconsistencies in the native SMAP retrievals partitioned by region and confirmed that the ensemble model could better refine the original coarse product and homogenize the results with the ground observations across the entire study area.

4.3. SM downscaling

The downscaled SM data produced by the optimized ensemble model for both the shallow and deep regions are illustrated in Fig. 8. The first line shows a comparison between the original 9-km SMAP SSM retrievals and the estimated downscaled to 30 m for the entire Central Valley from November 1 to December 5, 2023. Similarly, the second line contrasts the 9-km native SMAP root-zone product against the downscaled 30-m RZSM map for the same time frame.

The SSM map depicts typical patterns across the entire Central Valley. The eastern region near the Sierra Nevada Mountain range exhibits lower values of approximately 0.1 cm^3/cm^3, as expected, owing to the rain-shadow effect in this region. Moreover, the moisture levels range from 0.15 to 0.22 cm^3/cm^3 throughout most of the northern region,

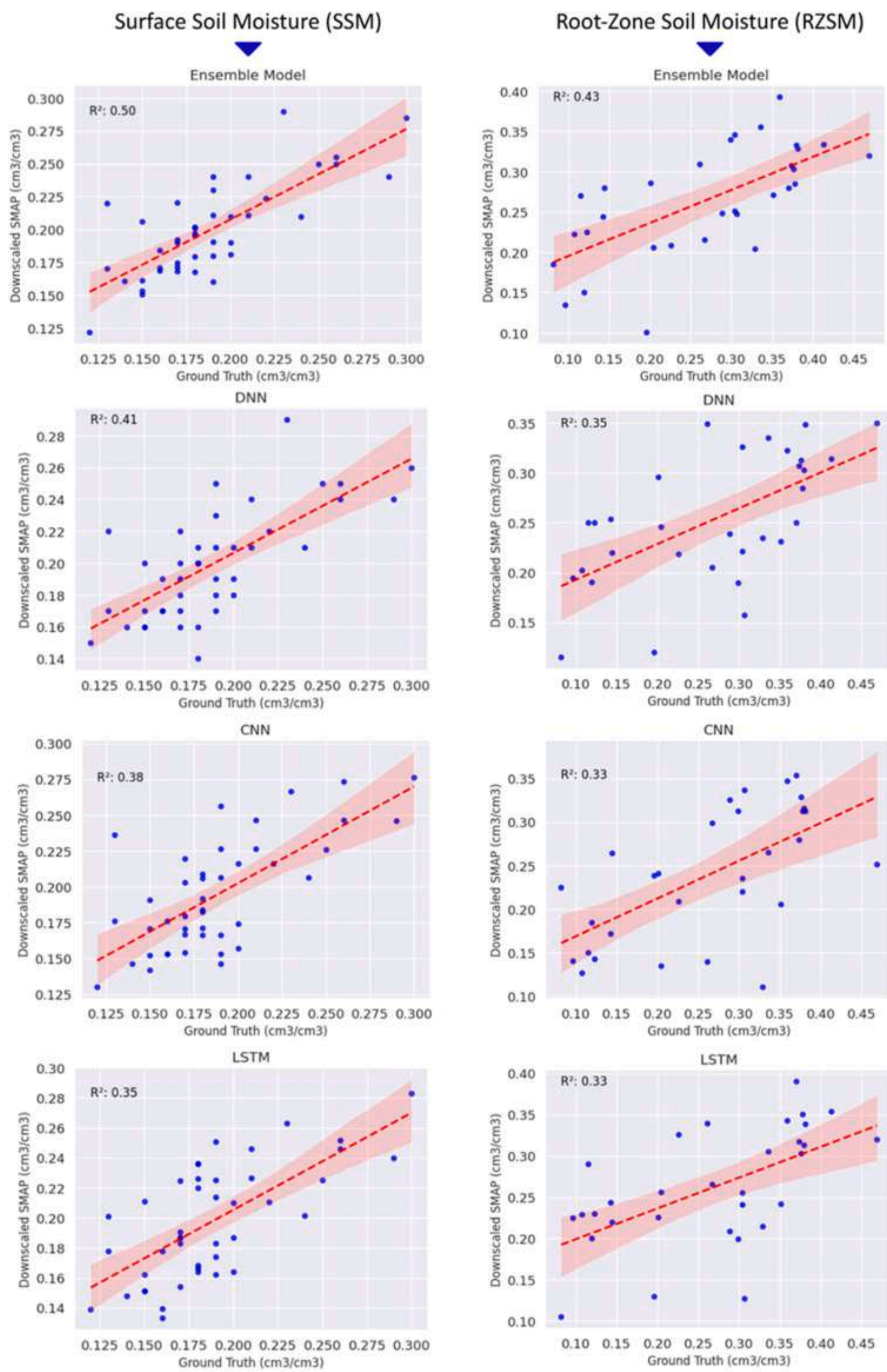

Fig. 6. Scatter plots of the observed and downscaled surface soil moisture (SSM) and root zone soil moisture (RZSM) data.

where agricultural activity is prominent, and precipitation has a significant effect on SSM. However, the SSM in the southern region exhibits higher variability, with readings ranging from 0.08 to 0.2 cm^3/cm^3 amid the heterogeneous cropland mosaics. Noticeable inconsistencies that are present in clustered pixels of the original SMAP with high SSM values are due to the model's design, aimed at capturing spatial correlations and trends, which may result in smoothing effects that reconcile variations across pixel clusters.

By contrast, the RZSM distributions show a lower congruence with the surface conditions, with the western Sierra Nevada foothills exhibiting relatively low values of approximately 0.18 cm^3/cm^3 on average. Additionally, the SSM levels in the northern region range from 0.08 to 0.12 cm^3/cm^3, indicating drier subsoil conditions, whereas the soils in the south are moderately more humid with SSM levels near 0.15 cm^3/cm^3, probably owing to the residual effects of in-season irrigation, with enhanced heterogeneity evident at finer scales. This clarifies the deeper

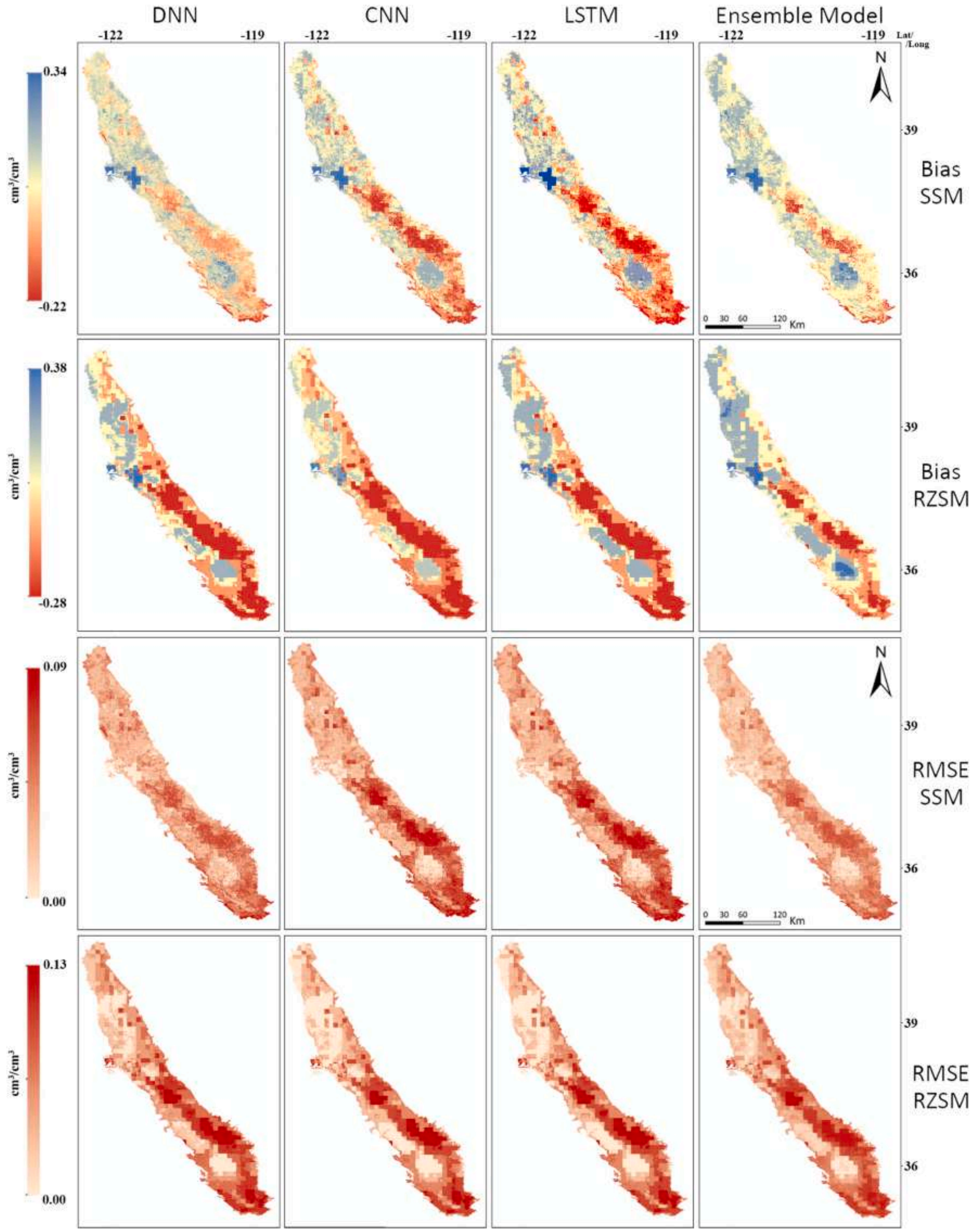

Fig. 7. Comparisons of the spatial patterns of bias and RMSE between the original Soil Moisture Active Passive (SMAP) product and 30 m-resolution downscaled maps.

moisture distributions with improved resolution of heterogeneities driven by the physical characteristics of subsurface soil, precipitation infiltration, and vegetation water use across various landscapes.

To further compare the downscaling results of each model, the spatial differences in the SM of two typical areas in the Central Valley are highlighted in Fig. 9. This visualization provides a localized context to complement the complete mapping of the entire study region obtained through each model, as shown in Fig. S7.

The detailed illustrations in Fig. 9 reveal valuable subtleties in the SM data simulated by the models at localized scales. For the first region, the CNN exhibits different patterns than the other models for near-surface conditions, whereas in the second region, the representation of DNN diverges slightly for the deeper layer, whereas that of the CNN again stands out. However, the ensemble model clearly exhibits the finer textural characteristics of the SSM that align with the landscape features, suggesting that it best captures the finer spatial gradients. Although the results of the models were generally in agreement, some of the CNN models exhibited some localized discrepancies, resulting in abnormal patterns. However, the ensemble model accurately reflected the relationship between the SM and the landscape features under

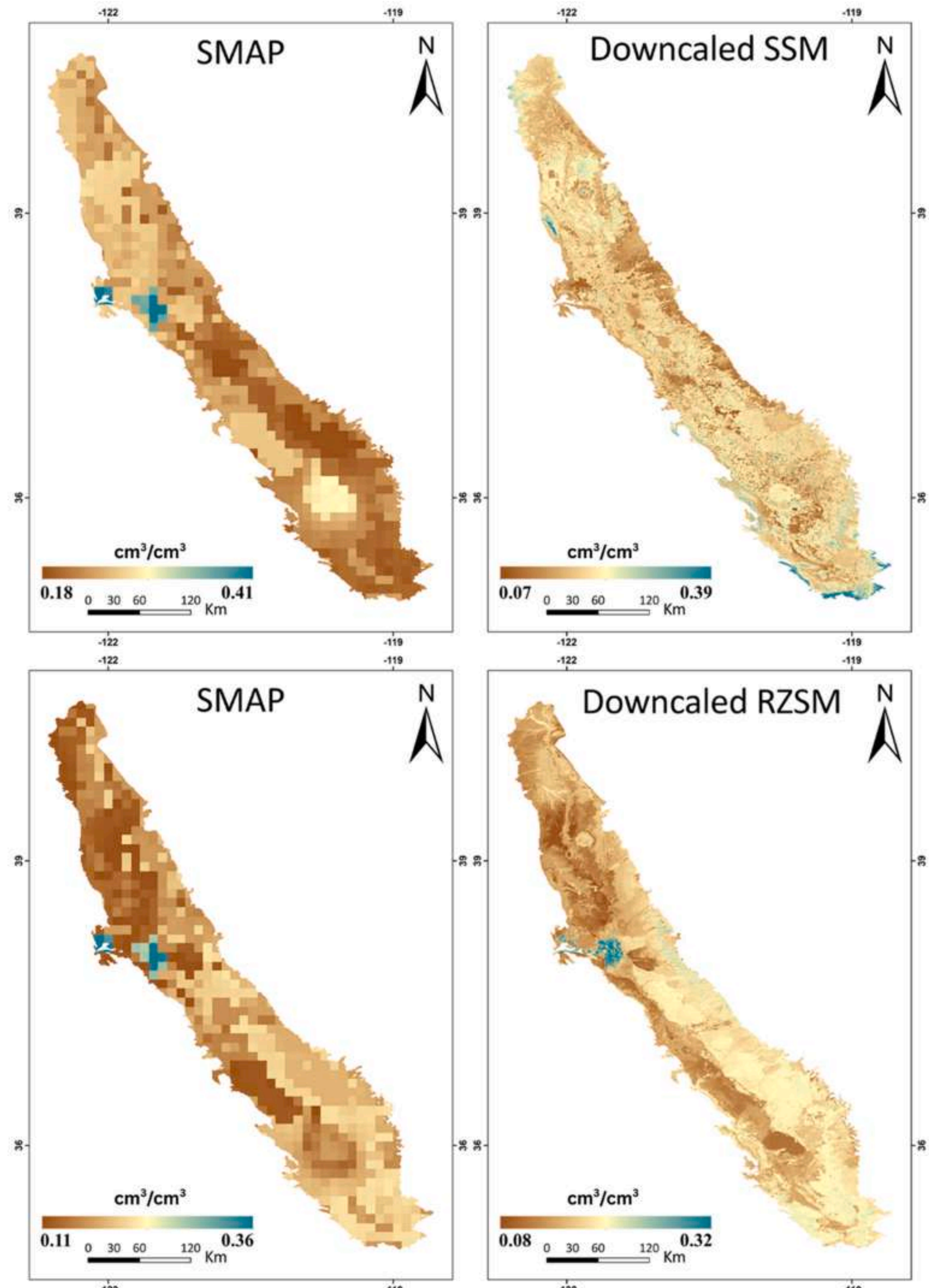

Fig. 8. Comparison of the original 9-km Soil Moisture Active Passive (SMAP) data with the ensemble model downscaled 30-m maps for surface soil moisture (SSM) and root-zone soil moisture (RZSM) across the entire Central Valley.

different magnifications.

4.4. Analysis of seasonal changes in SM

To analyze the seasonal changes in SM across the Central Valley during 2023, Fig. 10 compares the downscaled SSM and RZSM maps for the four main seasons.

Fig. 10 shows the distinct spatiotemporal patterns of SM corresponding to seasonal climate conditions. Evidently, during spring, the SSM across most of the valley was high, as soils recharged following the wet winter months. However, some parts of the southern valley exhibited drier surface conditions than those in the north, and the RZSM was more uniformly moist in the north.

In the summer, both the SSM and RZSM deficits increased substantially, with most areas exhibiting moisture levels below 50 %. Additionally, drier conditions prevailed as the amount of water lost via ET exceeded that provided by precipitation. The southeastern valley experienced the most severe drying at both the shallow and deep depths. Additionally, the summer SM is affected by irrigation from groundwater, as shown in Fig. 8, wherein the eastern region of the San Joaquin Valley appears wetter than the western region, which does not have sufficient groundwater for irrigation. Moreover, the western region depends on surface water deliveries from the north, which can be curtailed during dry periods.

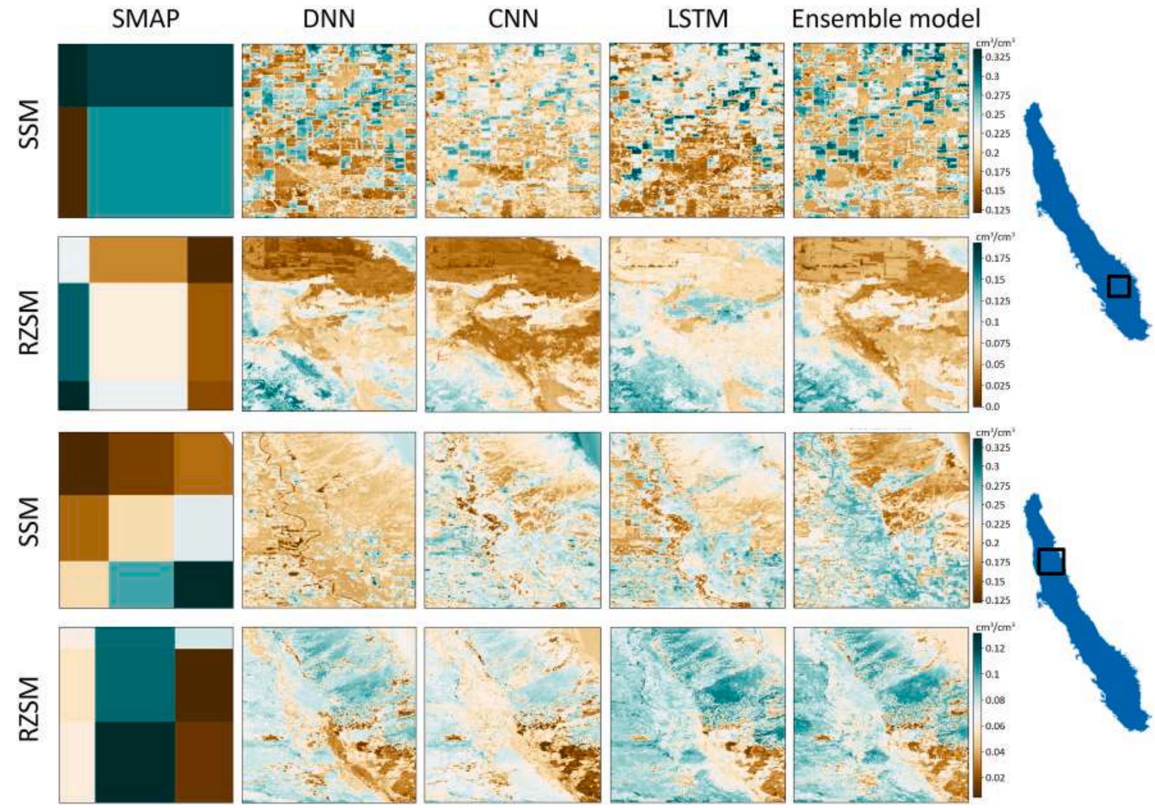

Fig. 9. Detailed illustrations of the downscaled Soil Moisture Active Passive (SMAP) results in two typical regions of the Central Valley.

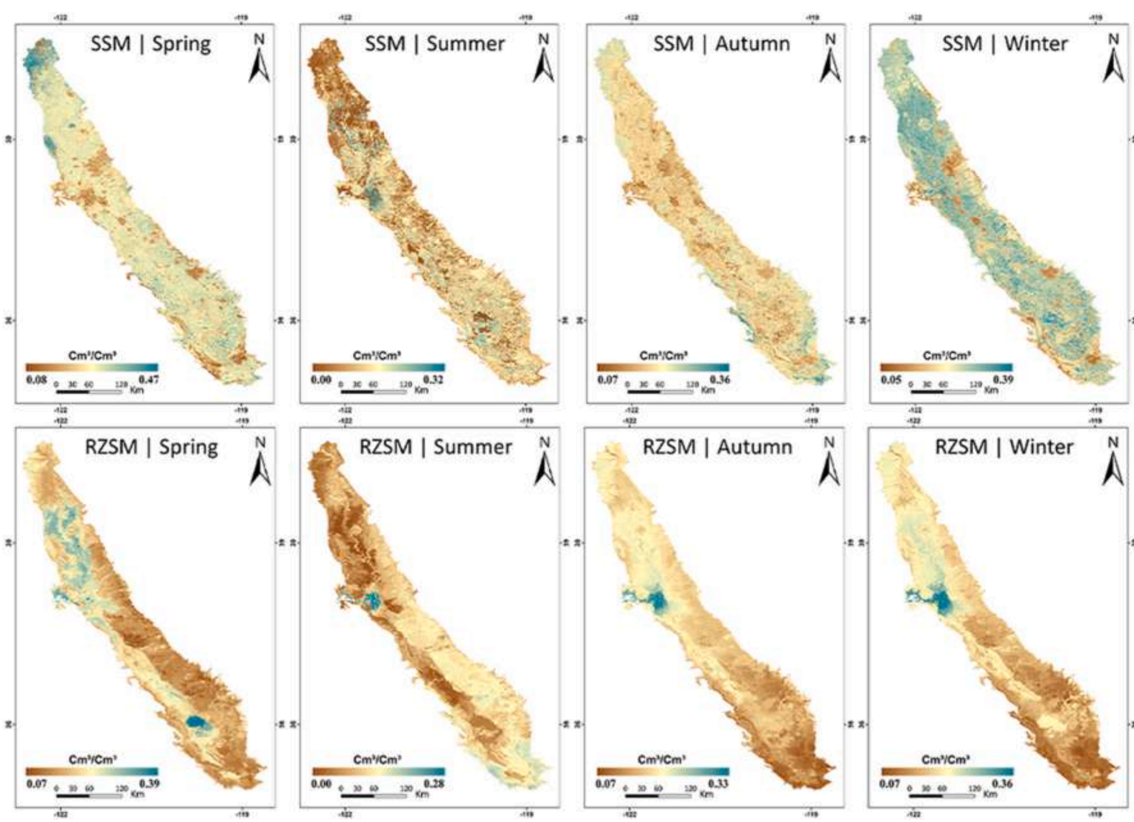

Fig. 10. Seasonal spatial patterns in downscaled (from 9 km to 30 m) surface soil moisture (SSM) and root-zone soil moisture (RZSM) maps across the Central Valley from May 2023 to March 2024.

Precipitation increased during the fall and temperatures cooled, allowing for partial recovery of moisture levels toward wetter winter conditions. However, the spatial variability increased as the SM levels in the southern regions recovered slightly less than those in the northern regions. Additionally, the RZSM responded more gradually to rainfall in the San Joaquin Valley than in the Sacramento Valley.

The plant-available water content at the end of the winter was evaluated using the ensemble downscaled RZSM as shown in (Fig. 11). The AWC map revealed distinct spatial patterns across the Central Valley, reflecting the combined influence of soil properties and spatial variability in rainfall.

Subsequently, winter replenished SSM levels in most of the Central Valley due to California's Mediterranean-type climate. RZSM levels increased across most of the Central Valley, but the rise was least pronounced in the Westside and southern regions of the San Joaquin Valley, where the rain shadow effect from the coastal mountains along the valley's western edge limited precipitation. Thus, Fig. 10 illustrates the pronounced seasonal cyclicality of SM, driven by changes in temperature, precipitation, evapotranspiration, and irrigation across the croplands of the Central Valley. Analysis of the available water content at the end of winter showed consistently higher values along the eastern edge of the Central Valley, adjacent to the Sierra Nevada mountains, particularly in the Sacramento Valley region (Fig. 11).

To demonstrate the downscaled SM products' ability to capture the fine-scale variability of SM, Fig. 12 illustrates the seasonal changes in the young pistachio orchard, which comprised two fields: one with a cover crop (a mix of triticale and vetch) and another without it.

The results show that the general seasonal trends exhibited by the in-situ neutron probe measurements were captured well by the model, albeit with some deviations. For the cover-crop field, the model accurately reproduced the soil-wetting pattern from September to March, demonstrating higher moisture levels than those in the field with no cover crop. This suggests that the downscaling approach can detect the SM moderating effects of cover crops. However, some overestimations

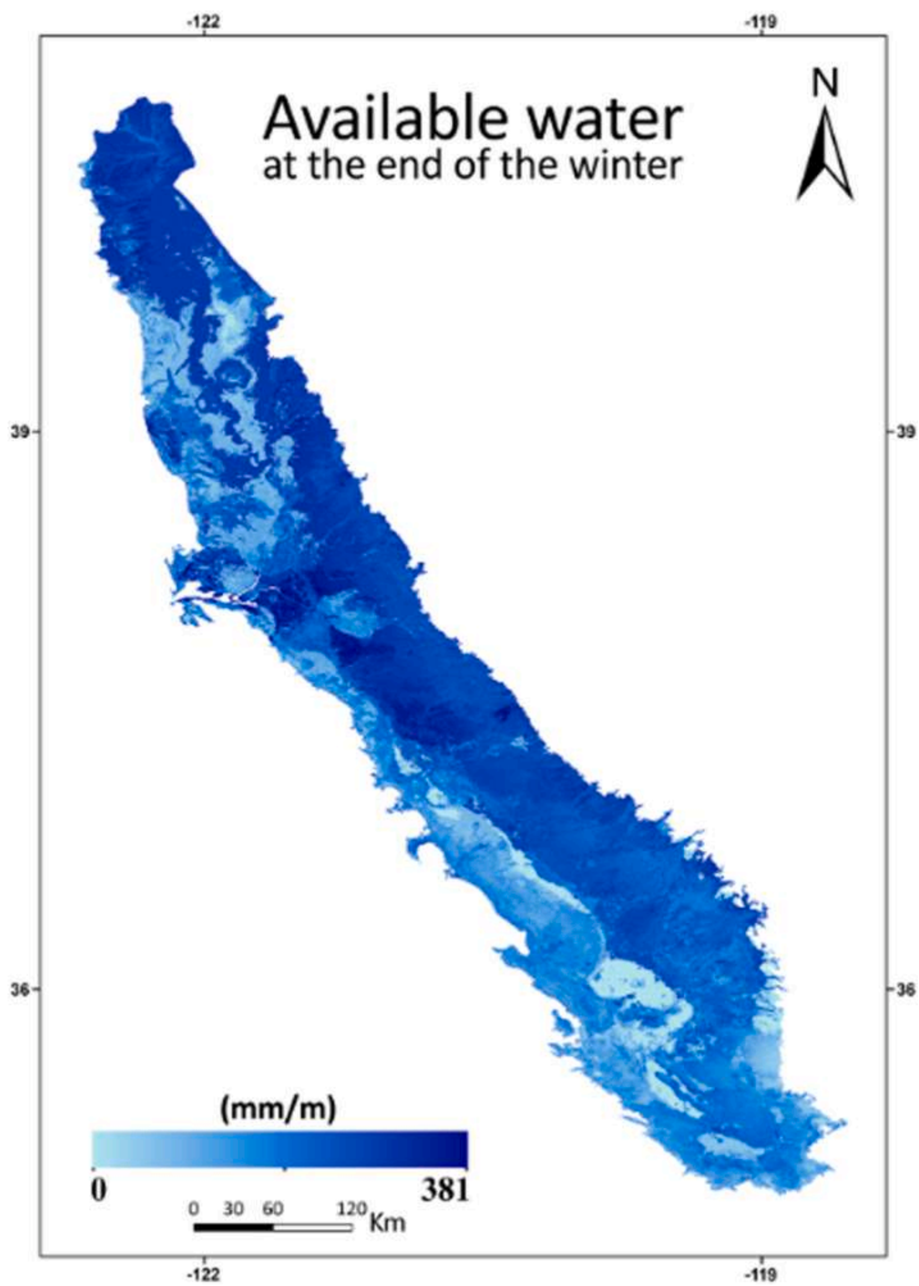

Fig. 11. Spatial variability in plant available water at the end of the winter season 2023 in the Central Valley of California, at 30 m spatial resolution.

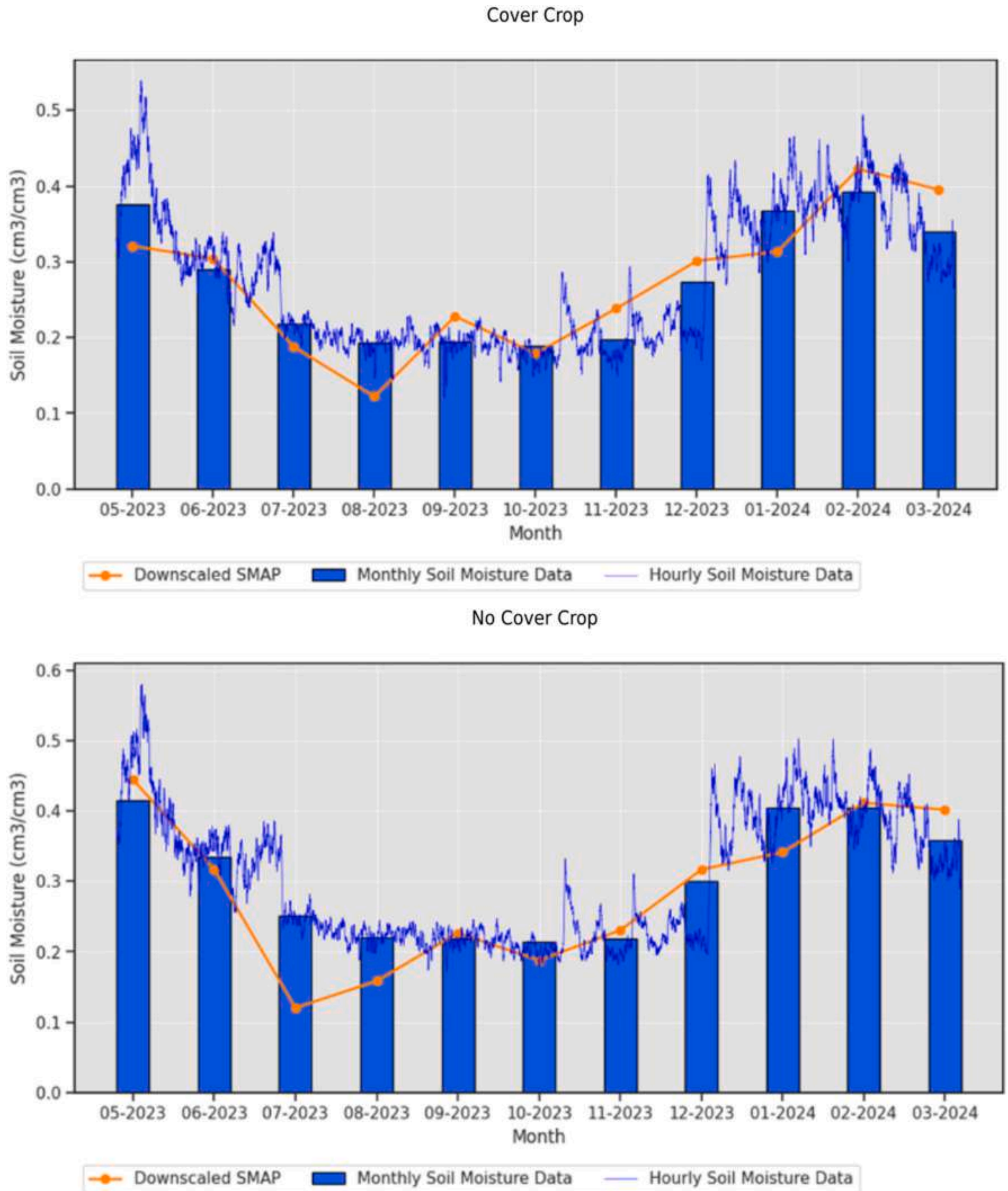

Fig. 12. Monthly variations in downscaled soil-moisture (SM) data versus the observed in-situ values in the young pistachio orchard. SMAP: Soil Moisture Active Passive.

(approximately 0.05 cm^3/cm^3) were evident for the spring and fall months when transitioning between wet and dry periods. Additionally, the SM during drier conditions in July and August was underestimated by approximately 0.03–0.07 cm^3/cm^3, potentially reflecting the model's limitations in resolving the effect of micro irrigation on the SM dynamics. Although not a perfect match, the downscaled data sufficiently represented the impact of cover cropping on SM availability throughout the year.

The results for the field with no cover crop similarly captured the seasonal cycles, exhibiting a closer agreement of approximately 0.01–0.03 cm^3/cm^3 with the data from September to March. However, an overestimation of approximately 0.09 cm^3/cm^3 occurred under wet conditions in May, and the drying during July was underestimated by approximately 0.08 cm^3/cm^3. The SSM layer of this field remained slightly wetter, reflecting a lack of water use by the cover crop. Although not perfect, the downscaled SMAP data can be useful for monitoring seasonal soil conditions, with implications for irrigation and water allocation management in over-drafted groundwater basins.

5. Discussion

5.1. Model construction

Downscaling coarse-resolution satellite observations to finer spatial scales is crucial for enabling more comprehensive investigations and applications in domains such as hydrology, agriculture, and climate science. The sensitivity analysis provided further insights into the role of different predictors in shaping soil moisture patterns at varying depths. For Surface Soil Moisture (SSM), precipitation (CHIRPS), elevation (DEM), and vegetation indices (NDVI, NDWI, SAVI) were the most influential predictors, as their exclusion caused the largest increase in RMSE (>0.15 cm^3/cm^3). Radar backscatter (VH, VV), evapotranspiration, and land-surface temperature contributed more modestly, reflecting secondary effects of surface roughness and energy balance. In contrast, Root-Zone Soil Moisture (RZSM) was primarily governed by soil texture and organic-matter content, with their removal producing the highest RMSE (0.15–0.25 cm^3/cm^3). Precipitation and elevation also exerted a measurable influence, whereas vegetation and climatic factors played a lesser role. These depth-dependent sensitivities confirm that near-surface moisture is mainly driven by short-term hydrometeorological processes, while subsurface storage is more strongly shaped by lithologic and terrain controls.

The DNN and CNN models performed moderately well for SSM downscaling, aligning with previous studies (Xu et al., 2021, 2022; Fang et al., 2022; Fuentes et al., 2022). The LSTM model, which is commonly used for temporal predictions (Celik et al., 2022; Li et al., 2022), was employed as a feature extractor to encode spectral data, similar to CNN, and its performance was on par with that of the CNN for this regression downscaling task. Interestingly, the results indicated that the 1D CNN is well-suited for downscaling spectral SM data. This targeted 1D structure avoids potential issues arising when using sequential data (Kim et al., 2022; Tamang et al., 2023). Moreover, the additional encoding of spatial information in 2D CNNs can introduce complexity and overfitting risks (Yang et al., 2021; Namdari et al., 2023), which are mitigated by the streamlined 1D approach that solely analyzes spectral data. Harnessing the advantages of a 1D CNN in this manner allows for capturing predictive relationships from remote sensing data while avoiding complexity that could reduce downscaling accuracy. The ensemble framework further enhanced performance, consistently achieving the highest correlations and lowest errors for both SSM and RZSM. Numerous studies have demonstrated similar improvements by employing ensembles of DL models, regression techniques, and other data-fusion approaches (Abbaszadeh et al., 2019; Zhang et al., 2022; Yang et al., 2023). The optimized custom architecture developed in this study represents an advancement in state-of-the-art architectures by integrating individual DNN, CNN, and LSTM models within a constrained and efficient 1D CNN structure.

To deal with the inherent mismatch of spatial resolution between the downscaled SM data and the in-situ measurement, we applied a depth- and footprint-aware matching approach to leverage the strength of each sensing method and to match them to surface and RZSM. These matching strategies aimed to reduce scale mismatch errors; however, representativeness errors remain a significant source of uncertainty, particularly for point-based sensors in heterogeneous landscapes (Crow et al., 2012; Gruber et al., 2020). For example, CRNP's larger spatial footprint inherently smooths small-scale variability, potentially resulting in lower observed bias or RMSE relative to sensors like TDR, which are more sensitive to micro-scale soil and vegetation heterogeneity (Bogena et al., 2013). These differences underscore the need for careful interpretation of validation statistics across sensor types. Our results reflect these nuances, with the comparison error characteristics influenced not only by the accuracy of the downscaling model but also by the spatial representativeness of the reference data used.

5.2. Temporal stability

Reliable temporal SM dynamics are crucial for monitoring agriculture, and downscaling must preserve native time-series behavior. Recent studies on data downscaling have also analyzed temporal stability when evaluating model performance. Yin et al. (2023) examined the spatio-temporal heterogeneity and stability of a model used for downscaling the SM data of the Heihe River Basin from 2020 and reported standard deviations ranging from 0 to 0.13, representing modest seasonal variation. However, Qu et al. (2021), observed seasonal fluctuations in the spatial correlation (R-spatial) between downscaled and in-situ SM, especially in wet periods, indicating downscaling affects R-spatial more than coarse data. Additionally, Nasta et al. (2018) found that downscaled field-scale SM showed high temporal stability during wet seasons, greater interannual variability in spring, and lowest stability in summer due to solar-driven hillslope patterns. Our results align with these findings, capturing stable wet-season SM patterns and seasonal fluctuations during transitions.

5.3. Implication for agricultural water management

The study highlights the potential to store substantial plant-available water in the root zone after a normal or wet winter. For 6 million irrigated acres in the Central Valley, an average of 190.5 mm of available water at winter's end translates to 3.75 million acre-ft (4.6 km^3) for crop use if managed properly. This supports Devine and O'Geen (2019), who reported 17–36 km^3 of soil water storage contributing to crop use over 13 years, and showed that climate-smart practices like delayed spring irrigation and deeper, less frequent watering can reduce irrigation needs. Effective use, however, requires careful early-season depletion management.

The study produced high-resolution maps of end-of-winter available water, which are critical for agricultural water management under groundwater sustainability regulations. Groundwater Sustainability Agencies can use these maps to estimate evapotranspiration of applied water and monitor grower allocations under SGMA. Growers can also leverage this information to optimize irrigation timing, particularly by delaying early-spring applications to reduce water use, as supported by previous studies (Devine and O'Geen, 2019; Shackel et al., 2021; Waqas et al., 2021). The observed spatial variability in available water, including sharp regional differences, highlights that ET_{aw} requirements can vary substantially across the Central Valley, even for the same crops, due to differences in precipitation, soil properties, and local management practices.

5.4. Limitations and future research

While this study focused on evaluating the performance of selected deep learning architectures for downscaling SMAP soil moisture data, it represents an initial exploration rather than an exhaustive evaluation of all possible modeling approaches. Future work could broaden this investigation by incorporating additional DL architectures, benchmarking them against both traditional statistical and physically based models, and exploring transferability across different climate regimes. Furthermore, he integration of physical models remains essential since they incorporate an understanding of physical processes. Therefore, future studies should develop a hybrid framework that combines DL with a process-based hydrological or land-surface model. Incorporating physical constraints and representations of flow pathways may also help address errors and improve both spatial and temporal consistencies. The ability of process models to extrapolate to new conditions may also be enhanced by integrating big data-driven DL models.

There are several promising avenues for future research in this area. A key direction involves conducting spatiotemporal analyses over long multidecadal timeframes, as opposed to a single season. SM is a nonstationary variable that is sensitive to climate change. Therefore, analyzing patterns over several decades in major agricultural regions, such as California's Central Valley, could provide new insights into various dynamics, such as drought onset and recovery, and this information can be directly employed for drought monitoring and management. Furthermore, improved characterization of spatial and temporal SM variability can further enhance hydrological modeling to assess water-resource availability and risks under future climate-change scenarios. Therefore, advancements in modeling complex seasonal to multiyear SM patterns can potentially strengthen the resilience of agricultural and water-resource systems to climatic extremes.

6. Conclusion

This study developed and validated an optimized DL ensemble modeling framework for downscaling coarse-resolution SMAP SSM and RZSM data of California's agriculturally important Central Valley region to a resolution of 30 m. The proposed ensemble modeling addressed the limitations of individual models (DNN, CNN, and LSTM) by synthesizing their complementary strengths to improve the representation of spatiotemporal SM patterns and dynamics and achieving R = 0.789 and RMSE = 0.028 cm^3/cm^3 for SSM, and R = 0.683 and RMSE = 0.081 cm^3/cm^3 for RZSM. Sensitivity analysis further revealed that precipitation, topography (DEM), vegetation indices (NDVI, NDWI), and soil properties (organic matter, silt content) were the most influential drivers of downscaling accuracy. The refined multiscale training procedure helped overcome the scale-effect uncertainties by incorporating scale-dependent behaviors between resolutions. A comparison of localized in-situ networks demonstrated that the model reliably reproduced the intra-annual SM trends across seasons. The study then used high-resolution ensemble RZSM to estimate available water at the end of winter, which is important for determining evapotranspiration of applied water and refining delayed irrigation decisions.

This study represents a significant advancement in the field of spatial downscaling of soil moisture by employing a specialized ensemble DL model to downscale the data of highly managed agricultural regions based on sensitivity and uncertainty analyses of land-surface parameters. Facilitating enhanced understanding and monitoring of seasonal soil conditions at a fine scale can help enhance agricultural and water-resource resilience in water-limited environments under severe climate-change conditions. Future studies should incorporate physical constraints, conduct multi-decadal analysis, and integrate hydrological modeling to strengthen the physical realism of predictions, enhance the interpretability of machine learning outputs, and support more robust landscape and water-resource management under diverse climatic and land-use scenarios.

Beyond enhancing spatial resolution, this study also provides insights into the spatial drivers of soil moisture and demonstrates how deep learning can effectively disentangle multiscale, nonlinear dependencies that are often missed by traditional methods.

CRediT authorship contribution statement

Ali Azedou: Writing – original draft, Visualization, Validation, Software, Methodology, Investigation, Formal analysis, Conceptualization. **Aouatif Amine:** Writing – review & editing, Supervision, Investigation. **Said Lahssini:** Writing – review & editing, Supervision, Investigation. **Gordon Osterman:** Writing – review & editing, Investigation. **Mauricio Arboleda-Zapata:** Writing – review & editing, Investigation. **Michael Cosh:** Writing – review & editing. **Isaya Kisekka:** Writing – review & editing, Visualization, Supervision, Methodology, Investigation, Funding acquisition, Formal analysis, Conceptualization.

Funding

This study was supported by the USDA NIFA Award [number 2021-68012-35914] and the US-MoroccoFulbright Fellowship program.

Declaration of competing interest

The authors declare that they have no known competing financial interests or personal relationships that could have appeared to influence the work reported in this paper.

Acknowledgments

We are grateful to the students who supported the data collection at the various study sites and to Dr. Jan Hopmans for reviewing the manuscript before submission.

Appendix A. Supplementary data

Supplementary data to this article can be found online at https://doi.org/10.1016/j.envsoft.2025.106824.

Data availability

Shared a link to the Github repository. Link: https://github.com/itsaliaze/SMAP-Downscaling.git.

References

Abbaszadeh, P., Moradkhani, H., Zhan, X., 2019. Downscaling SMAP radiometer soil moisture over the CONUS using an ensemble learning method. Water Resour. Res. 55, 324–344. https://doi.org/10.1029/2018WR023354.
Abelen, S., Seitz, F., Abarca-del-Rio, R., Güntner, A., 2015. Droughts and Floods in the La Plata Basin in Soil Moisture Data and GRACE. Remote Sens. 7, 7324–7349. https://doi.org/10.3390/rs70607324.
Alemu, W.G., Henebry, G.M., Melesse, A.M., 2019. Land surface phenologies and seasonalities in the US prairie pothole region coupling AMSR passive microwave data with the USDA cropland data layer. Remote Sens. 11, 2550.
Anbarasu, S., Brindha, K., Elango, L., 2020. Multi-influencing factor method for delineation of groundwater potential zones using remote sensing and GIS techniques in the western part of perambalur district, southern India. Earth Sci Inform 13, 317–332. https://doi.org/10.1007/s12145-019-00426-8.
Azedou, A., Amine, A., Kisekka, I., et al., 2023. Enhancing land cover/land use (LCLU) classification through a comparative analysis of hyperparameters optimization approaches for deep neural network (DNN). Ecol. Inform. 78, 102333. https://doi.org/10.1016/j.ecoinf.2023.102333.
Babaeian, E., Sadeghi, M., Jones, S.B., et al., 2019. Ground, proximal, and satellite remote sensing of soil moisture. Rev. Geophys. 57, 530–616. https://doi.org/10.1029/2018RG000618.
Babbitt, C.H., Gibson, K.E., Sellers, S., et al., 2018. The Future of Groundwater in California: Lessons in Sustainable Management from Across the West.
Bell, J.P., 1987. Neutron Probe Practice.
Bogena, H.R., Huisman, J.A., Baatz, R., et al., 2013. Accuracy of the cosmic-ray soil water content probe in humid forest ecosystems: the worst case scenario: cosmic-ray probe in humid forested ecosystems. Water Resour. Res. 49, 5778–5791. https://doi.org/10.1002/wrcr.20463.
Brown, C.F., Brumby, S.P., Guzder-Williams, B., et al., 2022. Dynamic world, near real-time global 10 m land use land cover mapping. Sci. Data 9, 251.
Carranza, C., Nolet, C., Pezij, M., van der Ploeg, M., 2021. Root zone soil moisture estimation with random forest. J. Hydrol. 593, 125840. https://doi.org/10.1016/j.jhydrol.2020.125840.
Celik, M.F., Isik, M.S., Yuzugullu, O., et al., 2022. Soil moisture prediction from remote sensing images coupled with climate, soil texture and topography via deep learning. Remote Sens. 14, 5584. https://doi.org/10.3390/rs14215584.
Chan, J.Y.-L., Leow, S.M.H., Bea, K.T., et al., 2022. Mitigating the multicollinearity problem and its machine learning approach: a review. Mathematics 10, 1283. https://doi.org/10.3390/math10081283.
Chan, S.K., Bindlish, R., O'Neill, P.E., et al., 2016. Assessment of the SMAP passive soil moisture product. IEEE Trans. Geosci. Rem. Sens. 54, 4994–5007. https://doi.org/10.1109/TGRS.2016.2561938.
Chaney, N.W., Minasny, B., Herman, J.D., et al., 2019. POLARIS soil properties: 30-m probabilistic maps of soil properties over the contiguous United States. Water Resour. Res. 55, 2916–2938. https://doi.org/10.1029/2018WR022797.
Colliander, A., Reichle, R.H., Crow, W.T., et al., 2022. Validation of soil moisture data products from the NASA SMAP Mission. IEEE J. Sel. Top. Appl. Earth Obs. Rem. Sens. 15, 364–392. https://doi.org/10.1109/JSTARS.2021.3124743.
Crow, W.T., Berg, A.A., Cosh, M.H., et al., 2012. Upscaling sparse ground-based soil moisture observations for the validation of coarse-resolution satellite soil moisture products. Rev. Geophys. 50. https://doi.org/10.1029/2011rg000372.
Dejonge, K.C., Richard, A.G., Ayse, K., Thorp, K.R., Meetpal, K.S., Marek, G.W., Altenhofen, J., Amatya, D.M., Blankenau, P., Datta, S., Grabow, G., Hashem, A.A., Isaya, K., Kjaersgaard, J., Marek, T., Peters, T., Porter, D., Reba, M.L., Rudnick, D., Senay, G., Sharma, V., Sridhar, V., Sun, G., Taghvaeian, S., Trezza, R., Trout, T.J., 2025. Evapotranspiration terminology and definitions. J. Irrigat. Drain. Eng. 151 (5). https://doi.org/10.1061/JIDEDH.IRENG-10491, 10.1061/JIDEDH.IRENG-10491.
Deng, K.A.K., Petropoulos, G.P., Bao, Y., et al., 2022. An examination of the SMAP operational soil moisture products accuracy at the Tibetan Plateau. Remote Sens. 14, 6255. https://doi.org/10.3390/rs14246255.
Deshon, J.P., Niemann, J.D., Green, T.R., et al., 2020. Stochastic analysis and probabilistic downscaling of soil moisture in small catchments. J. Hydrol. 585, 124711. https://doi.org/10.1016/j.jhydrol.2020.124711.

Devine, S., O'Geen, A.T., 2019. Climate-smart management of soil water storage: statewide analysis of California perennial crops. Environ. Res. Lett. 14 (4), 044021.
DWR, 2021. Groundwater Demand Management.
Entekhabi, D., Njoku, E.G., O'Neill, P.E., et al., 2010. The soil moisture active passive (SMAP) mission. Proc. IEEE 98, 704–716. https://doi.org/10.1109/JPROC.2010.2043918.
Escriva-Bou, A., Hanak, E., Cole, S., Medellín-Azuara, J., 2023. The Future of Agriculture in the San Joaquin Valley. Public Policy Institute of California.
Fan, X., Liu, Y., Gan, G., Wu, G., 2020. SMAP underestimates soil moisture in vegetation-disturbed areas primarily as a result of biased surface temperature data. Rem. Sens. Environ. 247, 111914.
Fang, Y., Xu, L., Chen, Y., et al., 2022. A bayesian deep image prior downscaling approach for high-resolution soil moisture estimation. IEEE J. Sel. Top. Appl. Earth Obs. Rem. Sens. 15, 4571–4582. https://doi.org/10.1109/JSTARS.2022.3177081.
Fischer, S.C., Niemann, J.D., Scalia, J., et al., 2025. Assessing the influence of model inputs on performance of the EMT + VS soil moisture downscaling model for a large foothills region in northern Colorado. J. Hydrol. 650, 132397. https://doi.org/10.1016/j.jhydrol.2024.132397.
Fuentes, I., Padarian, J., Vervoort, R.W., 2022. Towards near real-time national-scale soil water content monitoring using data fusion as a downscaling alternative. J. Hydrol. 609, 127705. https://doi.org/10.1016/j.jhydrol.2022.127705.
Funk, C., Peterson, P., Landsfeld, M., et al., 2015. The climate hazards infrared precipitation with stations—a new environmental record for monitoring extremes. Sci. Data 2, 150066. https://doi.org/10.1038/sdata.2015.66.
Gaeta, G.M., 2021. A Program Proposal to Enhance Groundwater Recharge to Achieve Groundwater Sustainability in California. California State University, Bakersfield. Master's Thesis.
Glotfelty, T., Ramírez-Mejía, D., Bowden, J., et al., 2021. Limitations of WRF land surface models for simulating land use and land cover change in Sub-Saharan Africa and development of an improved model (CLM-AF v. 1.0). Geosci. Model Dev. (GMD) 14, 3215–3249.
Gruber, A., De Lannoy, G., Albergel, C., et al., 2020. Validation practices for satellite soil moisture retrievals: what are (the) errors? Rem. Sens. Environ. 244, 111806.
Gu, Z., Zhu, T., Jiao, X., et al., 2021. Neural network soil moisture model for irrigation scheduling. Comput. Electron. Agric. 180, 105801. https://doi.org/10.1016/j.compag.2020.105801.
He, C., Chen, F., Barlage, M., et al., 2023. Enhancing the community Noah-MP land model capabilities for Earth sciences and applications. Bull. Am. Meteorol. Soc. 104, E2023–E2029.
Holmes, R.T., 2023. Strategies for Managing Naturally Occurring Contaminants in Groundwater Basins of the Central Valley, California. Stanford University. PhD Thesis.
Howitt, R., Medellin-Azuara, J., Lund, J., MacEwan, D., 2014. Preliminary 2014 Drought Economic Impact Estimates in Central Valley Agriculture. Center for Watershed Sciences, University of California Davis Davis, California. https://watershed.ucdavis.edu/files/biblio/Preliminary_2014_drought_economic_impacts-05192014.pdf. (Accessed 10 July 2014).
Jiang, H., Shen, H., Li, H., et al., 2017. Evaluation of multiple downscaled microwave soil moisture products over the central Tibetan Plateau. Remote Sens. 9, 402. https://doi.org/10.3390/rs9050402.
Kim, H., Wigneron, J.-P., Kumar, S., et al., 2020. Global scale error assessments of soil moisture estimates from microwave-based active and passive satellites and land surface models over forest and mixed irrigated/dryland agriculture regions. Rem. Sens. Environ. 251, 112052. https://doi.org/10.1016/j.rse.2020.112052.
Kim, J., Lee, M., Han, H., et al., 2022. Case study: development of the CNN model considering teleconnection for spatial downscaling of precipitation in a climate change scenario. Sustainability 14, 4719. https://doi.org/10.3390/su14084719.
Kofidou, M., Stathopoulos, S., Gemitzi, A., 2023. Review on spatial downscaling of satellite derived precipitation estimates. Environ. Earth Sci. 82, 424. https://doi.org/10.1007/s12665-023-11115-7.
LaDochy, S., Witiw, M., 2023. Precipitation: too much or too little. In: LaDochy, S., Witiw, M. (Eds.), Fire and Rain: California's Changing Weather and Climate. Springer Nature, Switzerland, Cham, pp. 67–94.
Li, Q., Zhu, Y., Shangguan, W., et al., 2022. An attention-aware LSTM model for soil moisture and soil temperature prediction. Geoderma 409, 115651. https://doi.org/10.1016/j.geoderma.2021.115651.
Li, R., Ou, G., Pun, M., Larson, L., 2018. Evaluation of groundwater resources in response to agricultural management scenarios in the central valley, California. J. Water Resour. Plann. Manag. 144, 04018078. https://doi.org/10.1061/(ASCE)WR.1943-5452.0001014.
Lindner, T., Puck, J., Verbeke, A., 2022. Beyond addressing multicollinearity: robust quantitative analysis and machine learning in international business research. J. Int. Bus. Stud. 53, 1307–1314. https://doi.org/10.1057/s41267-022-00549-z.
May-Lagunes, G., Chau, V., Ellestad, E., et al., 2023. Forecasting groundwater levels using machine learning methods: the case of California's Central valley. J. Hydrol. X 21, 100161. https://doi.org/10.1016/j.hydroa.2023.100161.
Mazzariello, A., Albano, R., Lacava, T., et al., 2023. Intercomparison of recent microwave satellite soil moisture products on European ecoregions. J. Hydrol. 626, 130311. https://doi.org/10.1016/j.jhydrol.2023.130311.
Mei, Y., Mai, J., Do, H.X., et al., 2023. Can hydrological models benefit from using global soil moisture, evapotranspiration, and runoff products as calibration targets? Water Resour. Res. 59. https://doi.org/10.1029/2022WR032064 e2022WR032064.
Nadeem, A.A., Zha, Y., Shi, L., et al., 2023. Spatial downscaling and gap-filling of SMAP soil moisture to high resolution using MODIS surface variables and machine learning approaches over ShanDian river basin, China. Remote Sens. 15, 812. https://doi.org/10.3390/rs15030812.
Namdari, H., Haghighi, A., Ashrafi, S.M., 2023. Short-term urban water demand forecasting; application of 1D convolutional neural network (1D CNN) in comparison with different deep learning schemes. Stoch. Environ. Res. Risk Assess. https://doi.org/10.1007/s00477-023-02565-3.
Nasta, P., Penna, D., Brocca, L., et al., 2018. Downscaling near-surface soil moisture from field to plot scale: a comparative analysis under different environmental conditions. J. Hydrol. 557, 97–108. https://doi.org/10.1016/j.jhydrol.2017.12.017.
Orang, M.N., Snyder, R.L., Shu, G., et al., 2013. California simulation of evapotranspiration of applied water and agricultural energy use in California. J. Integr. Agric. 12, 1371–1388. https://doi.org/10.1016/S2095-3119(13)60742-X.
Park, N.-W., Kim, Y., Kwak, G.-H., 2019. An Overview of Theoretical and Practical Issues in Spatial Downscaling of Coarse Resolution satellite-derived Products, vol. 35, pp. 589–607. https://doi.org/10.7780/kjrs.2019.35.4.8.
Peddinti, S.R., Hopmans, J.W., Abou Najm, M., Kisekka, I., 2020. Assessing effects of salinity on the performance of a low-cost wireless soil water sensor. Sensors 20, 7041. https://doi.org/10.3390/s20247041.
Peng, J., Loew, A., Merlin, O., Verhoest, N.E.C., 2017. A review of spatial downscaling of satellite remotely sensed soil moisture. Rev. Geophys. 55, 341–366. https://doi.org/10.1002/2016RG000543.
Qu, Y., Zhu, Z., Montzka, C., et al., 2021. Inter-comparison of several soil moisture downscaling methods over the Qinghai-Tibet Plateau, China. J. Hydrol. 592, 125616. https://doi.org/10.1016/j.jhydrol.2020.125616.
Reichle, R., De Lannoy, G., Koster, R., et al., 2022. SMAP L4 Global 3-hourly 9 Km EASE-grid Surface and Root Zone Soil Moisture Geophysical Data. Version 7.
Rouf, T., Maggioni, V., Mei, Y., Houser, P., 2021. Towards hyper-resolution land-surface modeling of surface and root zone soil moisture. J. Hydrol. 594, 125945.
Running, S., Mu, Q., Zhao, M., 2021. MODIS/terra Net Evapotranspiration 8-day L4 Global 500m SIN Grid V061. NASA EOSDIS Land Processes Distributed Active Archive Center (DAAC) Data Set MOD16A2-061.
Sahaar, S.A., Niemann, J.D., 2020. Impact of regional characteristics on the estimation of root-zone soil moisture from the evaporative index or evaporative fraction. Agric. Water Manag. 238, 106225. https://doi.org/10.1016/j.agwat.2020.106225.
Sahoo, A.K., De Lannoy, G.J.M., Reichle, R.H., Houser, P.R., 2013. Assimilation and downscaling of satellite observed soil moisture over the little river experimental watershed in Georgia, USA. Adv. Water Resour. 52, 19–33. https://doi.org/10.1016/j.advwatres.2012.08.007.
Sanchez-Mejia, Z.M., Papuga, S.A., Swetish, J.B., et al., 2014. Quantifying the influence of deep soil moisture on ecosystem albedo: the role of vegetation. Water Resour. Res. 50, 4038–4053. https://doi.org/10.1002/2013WR014150.
Saxton, K.E., Rawls, W.J., 2006. Soil water characteristic estimates by texture and organic matter for hydrologic solutions. Soil Sci. Soc. Am. J. 70, 1569–1578. https://doi.org/10.2136/sssaj2005.0117.
Sbahi, S., Zidan, K., Ouazzani, N., et al., 2025. Machine learning-driven optimization of phosphorus removal in nature-based treatment systems. J. Water Proc. Eng. 75, 108038. https://doi.org/10.1016/j.jwpe.2025.108038.
Shackel, K., Fulton, A., Arnold, K., et al., 2021. Pulling the Trigger for the Start of Irrigation in the Spring: Too Much Too Soon for Walnuts? Sacramento Valley Orchard.
Shangguan, Y., Min, X., Shi, Z., 2023. Inter-comparison and integration of different soil moisture downscaling methods over the Qinghai-Tibet Plateau. J. Hydrol. 617, 129014. https://doi.org/10.1016/j.jhydrol.2022.129014.
Shrestha, P., Kurtz, W., Vogel, G., et al., 2018. Connection between root zone soil moisture and surface energy flux partitioning using modeling, observations, and data assimilation for a temperate grassland site in Germany. JGR Biogeosciences 123, 2839–2862. https://doi.org/10.1029/2016JG003753.
Sumner, D., 2014. Greenhouse Gas Mitigation Opportunities in California Agriculture.
Tamang, C.P., Paul, S., Kumar, D.N., 2023. Downscaling of GCM output using deep learning techniques. In: Timbadiya, P.V., Singh, V.P., Sharma, P.J. (Eds.), Climate Change Impact on Water Resources. Springer Nature, Singapore, pp. 13–28.
Tang, K., Zhu, H., Ni, P., 2021. Spatial downscaling of land surface temperature over heterogeneous regions using random forest regression considering spatial features. Remote Sens. 13, 3645. https://doi.org/10.3390/rs13183645.
Verhoest, N.E., Van Den Berg, M.J., Martens, B., et al., 2015. Copula-based downscaling of coarse-scale soil moisture observations with implicit bias correction. IEEE Trans. Geosci. Rem. Sens. 53, 3507–3521.
Victoria, A.H., Maragatham, G., 2021. Automatic tuning of hyperparameters using Bayesian optimization. Evolving Systems 12, 217–223. https://doi.org/10.1007/s12530-020-09345-2.
Walsh, D., Turner, P., Grunewald, E., et al., 2013. A small-diameter NMR logging tool for groundwater investigations. Groundwater 51, 914–926. https://doi.org/10.1111/gwat.12024.
Wang, C., Fu, B., Zhang, L., Xu, Z., 2019. Soil moisture–plant interactions: an ecohydrological review. J. Soils Sediments 19, 1–9. https://doi.org/10.1007/s11368-018-2167-0.
Wannasin, C., Brauer, C.C., Uijlenhoet, R., et al., 2021. Daily flow simulation in Thailand Part I: testing a distributed hydrological model with seamless parameter maps based on global data. J. Hydrol.: Reg. Stud. 34, 100794. https://doi.org/10.1016/j.ejrh.2021.100794.
Waqas, M.S., Cheema, M.J.M., Hussain, S., Ullah, M.K., Iqbal, M.M., 2021. Delayed irrigation: An approach to enhance crop water productivity and to investigate its effects on potato yield and growth parameters. Agric. Water Manag. 245, 106576.
Wu, J., Xia, L., On Chan, T., et al., 2022. Downscaling land surface temperature: a framework based on geographically and temporally neural network weighted autoregressive model with spatio-temporal fused scaling factors. ISPRS J. Photogrammetry Remote Sens. 187, 259–272. https://doi.org/10.1016/j.isprsjprs.2022.03.009.

Xu, M., Yao, N., Yang, H., et al., 2022. Downscaling SMAP soil moisture using a wide & deep learning method over the Continental United States. J. Hydrol. 609, 127784. https://doi.org/10.1016/j.jhydrol.2022.127784.
Xu, W., Zhang, Z., Long, Z., Qin, Q., 2021. Downscaling SMAP soil moisture products with convolutional neural network. IEEE J. Sel. Top. Appl. Earth Obs. Rem. Sens. 14, 4051–4062. https://doi.org/10.1109/JSTARS.2021.3069774.
Yang, X., Liu, R., Yang, M., et al., 2021. Incorporating landslide spatial information and correlated features among conditioning factors for landslide susceptibility mapping. Remote Sens. 13, 2166. https://doi.org/10.3390/rs13112166.
Yang, Z., He, Q., Miao, S., et al., 2023. Surface soil moisture retrieval of China using multi-source data and ensemble learning. Remote Sens. 15, 2786. https://doi.org/10.3390/rs15112786.
Yin, D., Song, X., Zhu, X., et al., 2023. Spatiotemporal analysis of soil moisture variability and its driving factor. Remote Sens. 15, 5768. https://doi.org/10.3390/rs15245768.
Zhang, X., Zhang, T., Zhou, P., et al., 2017. Validation analysis of SMAP and AMSR2 soil moisture products over the United States using ground-based measurements. Remote Sens. 9, 104. https://doi.org/10.3390/rs9020104.
Zhang, Y., Liang, S., Zhu, Z., et al., 2022. Soil moisture content retrieval from landsat 8 data using ensemble learning. ISPRS J. Photogrammetry Remote Sens. 185, 32–47. https://doi.org/10.1016/j.isprsjprs.2022.01.005.
Zhao, H., Li, J., Yuan, Q., et al., 2022. Downscaling of soil moisture products using deep learning: Comparison and analysis on Tibetan Plateau. J. Hydrol. 607, 127570. https://doi.org/10.1016/j.jhydrol.2022.127570.
Zreda, M., Shuttleworth, W.J., Zeng, X., et al., 2012. COSMOS: the cosmic-ray soil moisture observing system. Hydrol. Earth Syst. Sci. 16, 4079–4099.